Title

Cdt1 stabilizes kinetochore—microtubule attachments via an Aurora B kinase—dependent mechanism

Journal

Journal of Cell Biology, 217(10)

ISSN

0021-9525

Authors

Agarwal, Shivangi

Smith, Kyle Paul

Zhou, Yizhuo

et al.

Publication Date

2018-10-01

DOI

10.1083/jcb.201705127

JCB Journal of Cell Biology

ARTICLE

Cdt1 stabilizes kinetochore–microtubule attachments via an Aurora B kinase–dependent mechanism

Shivangi Agarwal[1], Kyle Paul Smith[1], Yizhuo Zhou[2], Aussie Suzuki[3], Richard J. McKenney[4], and Dileep Varma[1]

Robust kinetochore–microtubule (kMT) attachment is critical for accurate chromosome segregation. G2/M-specific depletion of human Cdt1 that localizes to kinetochores in an Ndc80 complex–dependent manner leads to abnormal kMT attachments and mitotic arrest. This indicates an independent mitotic role for Cdt1 in addition to its prototypic function in DNA replication origin licensing. Here, we show that Cdt1 directly binds to microtubules (MTs). Endogenous or transiently expressed Cdt1 localizes to both mitotic spindle MTs and kinetochores. Deletion mapping of Cdt1 revealed that the regions comprising the middle and C-terminal winged-helix domains but lacking the N-terminal unstructured region were required for efficient MT binding. Mitotic kinase Aurora B interacts with and phosphorylates Cdt1. Aurora B–phosphomimetic Cdt1 exhibited attenuated MT binding, and its cellular expression induced defective kMT attachments with a concomitant delay in mitotic progression. Thus we provide mechanistic insight into how Cdt1 affects overall kMT stability in an Aurora B kinase phosphorylation-dependent manner; which is envisioned to augment the MT-binding of the Ndc80 complex.

Introduction

Accurate chromosome segregation during mitosis is accomplished by the concerted function of the bipolar mitotic spindle and kinetochores (Westhorpe and Straight, 2013). In this process, mitotic cells inevitably confront a challenge to maintain robust kinetochore–microtubule (kMT) attachment despite dynamic instability generated by rapid polymerization (growth) and depolymerization (shrinkage) of microtubules (MTs; Joglekar et al., 2010; DeLuca and Musacchio, 2012). How this dynamic process of kMT coupling is accomplished and regulated in vertebrates is not well understood.

A highly conserved network of protein complexes, called the KMN (Knl1, Mis12, Ndc80) network, is the core interface that links spindle MTs to the kinetochores (Cheeseman et al., 2006; Cheeseman and Desai, 2008; Afreen and Varma, 2015). The N-terminal region of the Ndc80 complex, containing the calponin homology (CH) domain and positively charged tail domain of the Hec1 subunit, constitutes an essential MT-binding site (Varma and Salmon, 2012). The N-terminal region of Knl1 has also been shown to be necessary for MT binding (Cheeseman et al., 2006; Welburn et al., 2010; Espeut et al., 2012). Recently, an unprecedented mitotic role for human Cdt1, a well-established DNA replication licensing factor, was discovered (Varma et al., 2012; Pozo and Cook, 2016). The Hec1 loop domain that generates a flexible hinge in an otherwise rigid Ndc80 complex (Wang et al., 2008) has been shown to recruit Cdt1 to kinetochores by interacting with Cdt1's N-terminal region (Varma et al., 2012). Precise, high-resolution separation measurement (delta) analysis between the extreme N and C termini of Ndc80 revealed that the Ndc80 complex bound to Cdt1 maintains an extended conformation that serves to stabilize kMT attachments via an unknown mechanism (Varma et al., 2012). Thus, while substantial research has provided insights into the structural and mechanistic aspects of the "canonical" licensing function of Cdt1, how Cdt1 influences kMT attachments during mitosis remains unclear.

Besides Cdt1, the loop region of Hec1 also serves as a docking site for several other microtubule-associated proteins (MAPs) such as Dis1 (vertebrate homologue of chTOG) and Dam1 in yeast (Hsu and Toda, 2011; Maure et al., 2011; Schmidt and Cheeseman, 2011). In fact, in budding yeast, the Ndc80 and Dam1 complexes function synergistically to bind to MTs (Tien et al., 2010). Similarly, in vertebrates, the loop region has been reported to recruit the Ska complex (Zhang et al., 2012) that also interacts with MTs through the unique winged-helix domain (WHD) of the Ska1 subunit. Further, the Ndc80 complex increases the affinity of the

[1]Department of Cell and Molecular Biology, Feinberg School of Medicine, Northwestern University, Chicago, IL; [2]Department of Biochemistry and Biophysics, The University of North Carolina at Chapel Hill, Chapel Hill, NC; [3]Department of Biology, The University of North Carolina at Chapel Hill, Chapel Hill, NC; [4]Department of Molecular and Cellular Biology, University of California, Davis, Davis, CA.

Correspondence to Dileep Varma: dileep.varma@northwestern.edu.

Ska1 subunit for MTs by eightfold (Schmidt et al., 2012; Abad et al., 2014). These studies suggest that although the Ndc80 complex is critical for kMT-binding, other factors such as the Dam1 and Ska complexes are required to efficiently orchestrate kMT attachments and chromosome segregation.

The present study was thus undertaken to address critical outstanding questions surrounding the role of Cdt1 at kinetochores in stabilizing kMT attachments (Varma et al., 2012). These include (1) whether Cdt1 directly binds to MTs and (2) how Cdt1 is regulated for its mitotic function. Using several biochemical, biophysical, and cell biological approaches, we demonstrate that human Cdt1 can directly interact with MTs of the mitotic spindle. We further show that Cdt1 is a novel target for Aurora B kinase and that Aurora B–mediated phosphorylation of Cdt1 regulates its MT-binding properties, which in turn influence mitotic progression.

Results

Cdt1 directly binds to MTs in vitro

We had previously demonstrated that Cdt1 localizes to mitotic kinetochores, dependent on the loop domain of the Hec1 subunit of the Ndc80 complex. Further, using a novel RNAi-mediated knockdown approach and microinjection of a function-blocking Cdt1 antibody, we showed that perturbation of Cdt1 function specifically during mitosis led to unstable kMT attachments, culminating in a late prometaphase arrest (Varma et al., 2012). Moreover, high-resolution microscopic analysis suggested that in the absence of Cdt1, the coiled coil of the Ndc80 complex assumed a bent conformation and the complex was not able to make a full extension along the kMT axis (Varma et al., 2012). But how Cdt1 contributed to this mechanism and imparted kMT stability was unclear.

To investigate this mechanism systematically, we began by analyzing the structure of Cdt1, but since no high-resolution structures of full-length Cdt1 have been published, we first subjected the human Cdt1 amino acid sequence to at least 10 different secondary structure prediction algorithms that predict disordered regions. Although the consensus readily identified previously crystallized WHDs as being well folded, the N-terminal 93 aa were convincingly predicted to be at least ∼35% intrinsically disordered, in addition to the linker region between the two WHDs (Fig. 1 A). Homology models generated using three modeling programs reliably identified the winged-helix middle (WHM) and C-terminal (WHC) domains, while the N-terminal region (1–160) was consistently predicted to have only limited secondary structure elements in the absence of other binding partners (Fig. 1 B). The NMR solution structure (PDB ID: 2KLO) determined for the C-terminal 420–557 aa of *Mus musculus*, abbreviated as mCdt1, revealed that this region adopts a WHD conformation (Khayrutdinov et al., 2009) in addition to the other WHD in the middle of Cdt1 (172–368 aa) responsible for Geminin binding (Lee et al., 2004). The WHD has traditionally been implicated primarily as a DNA binding motif, but emerging evidence suggests that it could also serve as a protein–protein interaction domain (Khayrutdinov et al., 2009). In addition to the canonical three-helix bundles and antiparallel β-sheets, the Cdt1 WHC contains an additional helix (H4) at the C terminus (Fig. S1 A). Superimposition of the homology model for human Cdt1 fragment 410–546 aa (generated using Phyre2; Kelley et al., 2015) with the available NMR structure of an mCdt1 fragment showed an overlap with root mean square deviation of 1.038 Å, indicating that the 410–546 aa of human Cdt1 indeed conforms to a WHD (Fig. 1 B).

The presence of a central and a C-terminal WHD in human Cdt1 similar to the MT-binding domain of the Ska complex (Abad et al., 2014) prompted us to posit a new paradigm in which Cdt1 bound to the loop may directly bind to MTs to create an additional MT-attachment site for the Ndc80 complex and contribute to the robustness of kMT attachments. To test our hypothesis, we first evaluated the ability of Cdt1 to directly bind to MTs using in vitro assays.

Proteins with large disordered regions are generally characterized by rapid degradation (Vavouri et al., 2009). Indeed, challenges in purifying the full-length human Cdt1 from bacterial system were circumvented by the deletion of the 92-aa disordered stretch from its N terminus, which likely contributed to its degradation, reduced expression, and poor solubility. The Cdt1 protein was successfully purified with an N-terminal GFP fusion (abbreviated as Cdt1$^{92–546}$; Fig. 1, C and D) and was evaluated for its ability to bind to MTs in a copelleting assay. The Cdt1$^{92–546}$ (1 µM) was found to copellet efficiently with taxol-stabilized MTs (Fig. 1 E). This interaction with MTs is specific, as Cdt1 was not enriched in the pellet fraction in the absence of MTs. To determine the apparent MT-binding affinity of Cdt1$^{92–546}$, we varied the MT concentration and measured the Cdt1 concentration required for half-maximal binding. In this assay, the apparent dissociation constant (K_d) was determined to be 2.20 ± 0.87 µM (Fig. 1 F). Because the construct used in this assay was devoid of the first 92 aa, full-length (FL) Cdt1$^{1–546}$ was purified with a GST tag that was subsequently cleaved using Factor Xa, and the untagged Cdt1$^{1–546}$ was tested for its ability to bind to MTs. As expected, the full-length protein also bound to MTs (Fig. 1 E) with an affinity (2.29 ± 0.45 µM) similar to that of Cdt1$^{92–546}$ (Fig. 1 F), indicating that the first disordered 92 aa are dispensable for the MT-binding function of Cdt1. As controls, neither purified GFP nor GST proteins fractionated with MTs, substantiating the specificity of interaction (Fig. S1, B and C).

To map the Cdt1-MT interaction, deletion fragments within Cdt1$^{92–546}$ were generated (Fig. 1, C and D). Interestingly, neither of the N-terminal fragments, Cdt1$^{92–232}$ or Cdt1$^{92–410}$, cosedimented with MTs (Fig. 1, G and H). However, the smallest C-terminal fragment, Cdt1$^{410–546}$, did show MT binding, although its efficacy was reduced by ∼50% compared with Cdt1$^{92–546}$ (Fig. 1 I). Thus, we conclude that the C terminus of Cdt1 (410–546 aa) is necessary but not sufficient for MT binding.

We further tested the ability of Cdt1 deletions to bind to Hec1 in an in vitro blot overlay assay. In accordance with the previous study (Varma et al., 2012), our data show that although the N-terminal fragments, Cdt1$^{92–232}$ and Cdt1$^{92–410}$, were incompetent to sediment with MTs (Fig. 1 G); they interacted with Hec1 in this assay (Fig. 1 J). On the other hand, the Cdt1$^{410–546}$ that did bind MTs to some extent was not able to bind Hec1 (Fig. 1 J). GFP loaded as control bait protein was unable to bind Hec1 prey.

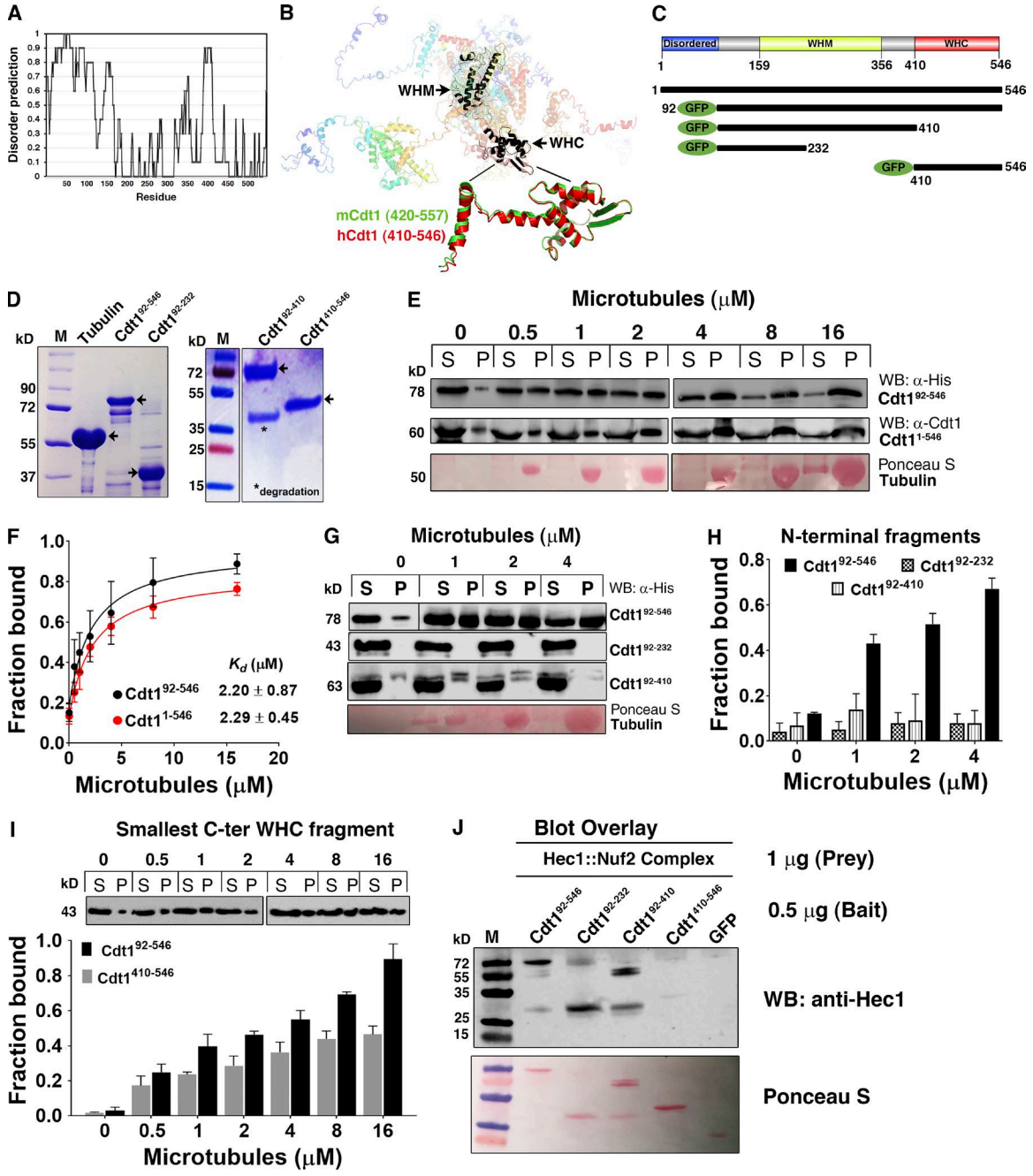

Figure 1. **Cdt1 is a novel MT-binding protein. (A)** Disorder prediction in human Cdt1. Disordered prediction (sum of 10 programs) is plotted as a function of residue number. **(B)** Seven homology models of full-length Cdt1; colored from N terminus (blue) to C terminus (red) with regions of low confidence or low overlap shown in translucent. Conserved WHM and WHC domains shown and aligned in gray and black, respectively, for clarity. Magnified is the PyMol rendered cartoon representation showing superimposition of the C-terminal human Cdt1 (410–546 aa, in red) generated using Phyre2 server with available NMR structure (PDB ID: 2KLO; in green) of mouse C-terminal Cdt1 (420–557 aa). **(C)** Constructs used in this study, full-length Cdt1 (1–546 aa), its deletion variant devoid of N-terminal 92 aa (92–546), and N- and C-terminal deletion variants generated in fusion with an N-terminal GFP tag for expression in bacteria are shown as black bars. Disordered domain shown in blue, WHM domain shown in yellow, and WHC domain shown in red. **(D)** SDS-PAGE (15%) of the indicated purified recombinant proteins along with native tubulin purified from porcine brain. M, molecular mass standard; *, degradation bands (confirmed by Western blot) in $Cdt1^{92–410}$. Arrows point toward the band corresponding to the protein of interest. **(E)** Western blots showing MT cosedimentation for $Cdt1^{92–546}$ (GFP-tagged) and full-length $Cdt1^{1–546}$ (without any tag), 1 µM each; purified from bacteria with the indicated concentrations of taxol-stabilized MTs (in µM). Samples fractionated as supernatant (S) and pellet (P) were analyzed by Western blot and probed with antibodies against 6×-His tag or anti-Cdt1 as indicated in each case to detect Cdt1. Ponceau S–stained tubulin. **(F)** Quantification (mean ± SD, $n = 3$) of the $Cdt1^{92–546}$ and $Cdt1^{1–546}$ blots using ImageJ. The 95% CI values obtained for the fit were 0.60–0.94 for B_{max}, 0.37–4.04 for K_d, and 0.07–0.29 for the background for the former construct; and 0.63–0.79 for B_{max}, 1.33–3.25 for K_d, and 0.08–0.18 for the background for the latter construct. **(G)** Representative Western blots of the binding of indicated deletion fragments to MTs in a cosedimentation assay with the indicated MT concentrations (top). **(H)** Quantification of binding (mean ± SD, $n = 3$) of the deletion fragments to MTs. **(I)** Quantification of MT-binding of Cdt1's smallest C-terminal fragment, $Cdt1^{410-546}$, and a representative Western blot (top) from three independent experiments (mean ± SD, $n = 3$). **(J)** Blot overlay assay to study Cdt1–Hec1 interaction. Indicated proteins (0.5 µg each) were loaded as bait on 18% SDS-PAGE gel, transferred to nitrocellulose

Cdt1 preferentially binds to straight MTs independent of the E-hook tails

At the C terminus of tubulin are negatively charged acidic tails of ∼20 aa, known as E-hooks, that represent a critical recognition site for many MT-binding proteins including Ndc80^{Bonsai} (Ciferri et al., 2008) and Dam1 (Ramey et al., 2011). The ability of Cdt1 to bind to MTs devoid of E-hooks was thus assessed in a cosedimentation assay. Similar to Ska1 (Abad et al., 2014) and chTOG (Spittle et al., 2000), Cdt1$^{92–546}$ did not show any appreciable reduction in its ability to bind to MTs lacking E-hooks (Fig. 2, A and B). This suggests that the critical contacts involved in this interaction might be the structured regions of tubulin monomers rather than the unstructured acidic tails. The highly basic nature of Cdt1 (predicted isoelectric point = 9.9) could be indicative of MT recognition through electrostatic/ionic interactions. Indeed, the binding of Cdt1$^{92–546}$ with MTs was substantially reduced to ∼50% in the presence of 250 mM NaCl (Fig. 2 C), suggesting that the binding may be at least partially electrostatic in nature.

Further, we assessed the preference for Cdt1 to bind to straight versus curved MTs. Unlike the CH domains of Ndc80 that bind to the dimeric tubulin interface and prefer a straight MT protofilament conformation, Ska accesses MTs by interacting with the structured regions within tubulin monomers independent of any conformation (Abad et al., 2014). The data revealed that even though MT binding was considerably reduced when the MTs were not straight, Cdt1 did retain the capacity to bind to curved MT protofilaments (Fig. S1, D–F), which may have important implications for the function of Cdt1 at the kMT interface in conjunction with the Ndc80 complex.

To test the preference of Cdt1 to bind to MT ends, polymerized MTs were sheared to increase the number of ends. We did not observe any significant increase in the association of Cdt1 with the MTs in this scenario (Fig. S1, D–F). This suggests that Cdt1 might not be merely a MT plus/minus end–specific protein, but that its binding sites are likely distributed along the length throughout the MT lattice.

Cdt1 diffuses on MTs in vitro and decorates mitotic spindles in vivo

To substantiate Cdt1-MT binding further, we directly visualized Cdt1$^{92–546}$ interaction with MTs using total internal reflection fluorescence microscopy (TIR-FM). The Cdt1$^{92–546}$ bound to Dylight405-labeled MTs at concentrations as low as 1 nM (Fig. 2 D) and started decorating the entire MT lattice at concentrations of ∼20 nM or higher (Fig. S1 G). In our conditions, individual molecules either bound statically or diffused along the MT lattice (Fig. 2 E). The dwell time distribution for Cdt1$^{92–546}$ on MTs was well described by a single exponential decay function yielding a characteristic dwell time (τ) of 2.37 s (Fig. 2 F). The calculated association rate (K_{on}, 10^{-6} $s^{-1} \cdot nM^{-1}$) was 1.07 ± 0.38, and the dissociation constant (K_d, μM) was 0.46 ± 0.17 (Fig. 2 F). A large fraction of Cdt1$^{92–546}$ (∼65%) was found to undergo short-range diffusive motion along the MT lattice to a moderate extent that falls in the range of 0–0.5 $\mu m^2/s$ (Fig. 2, G and E; and Video 1). A smaller fraction (∼20%) did not apparently diffuse at all, while an even smaller fraction (∼15%) exhibited relatively fast diffusion (>1 $\mu m^2/s$). The average diffusion coefficient for Cdt1$^{92–546}$ was ∼0.16 $\mu m^2/s$ under our experimental conditions (Fig. 2 G). Both Ndc80 and Ska complexes have also been shown to exhibit diffusion along the MT lattice, albeit at variable rates comparable to that observed for Cdt1 under our assay conditions (Schmidt et al., 2012; Zaytsev et al., 2015).

Although the in vitro experiments provide evidence that Cdt1 binds to MTs, we sought further evidence for this activity in cells. We had previously observed Cdt1 localization at mitotic kinetochores in paraformaldehyde-fixed LLCPK1 and PTK2 cells (Varma et al., 2012). We now show Cdt1 localization to kinetochores in HeLa cells using identical fixation conditions (Fig. 2 H). While Cdt1 transiently localized to the kinetochores predominantly during late prometaphase and metaphase (Fig. 2 H, panels i and ii), the detection dropped to almost negligible levels in anaphase and telophase (not depicted). Immunofluorescence staining of Cdt1 in methanol-fixed HeLa cells, which removed most of the kinetochore staining, allowed us to visualize clear mitotic spindle staining (Fig. 2 H). The variability observed in our previous (Varma et al., 2012) and present studies with respect to Cdt1 localization to kinetochores or spindle MTs is attributed to different antibodies, fixation conditions, and types of cells used.

To evaluate the spindle localization of Cdt1 comprehensively, HeLa cells were examined at different stages of mitosis. Anti-Cdt1 antibody staining substantially overlapped with the mitotic spindle, but individual spindle MT staining was often hard to discern. Cdt1 staining on spindles was intermittent, with areas of brighter or dimmer intensities, with maximum intensity observed at the spindle poles. Cdt1 spindle staining started to appear in late prometaphase after a majority of the chromosomes were aligned, with no evident MT staining during early or mid-prometaphase (not depicted). Cdt1 spindle staining was the brightest in metaphase (Fig. 2 H, panel iii). A low-magnification image with several cells demonstrating similar Cdt1 colocalization with spindle MTs during metaphase is shown (Fig. S1 H). In anaphase and telophase, Cdt1 MT staining is predominantly restricted to the spindle poles as discrete crescent-shaped structures that are brighter in anaphase compared with telophase (Fig. 2 H, panels iv–vi). No discernable Cdt1 localization to interpolar MTs or the MT bundles of the central spindle regions in anaphase or telophase was observed. Interestingly (but unexplainably as of now), Cdt1 staining at the cell periphery became prominent at the beginning of anaphase and in telophase, with moderately bright staining appearing at the regressing cleavage furrow (Fig. 2 H, panels v and vi). Faint Cdt1 colocalization was also observed in the condensing nuclei in late telophase, consistent with its G1 nuclear function (Fig. 2 H, panel vi).

membrane, and blocked with 5% SM-TBST. Hec1::Nuf2-His dimeric complex (1 μg; a generous gift from A. Desai and D. Cheerambathur, University of California, San Diego, La Jolla, CA) was overlaid as prey protein on the membrane for 12 h at 4°C. The blot was washed and probed with anti-Hec1 antibody (1:2,000; 9G3; Abcam) followed by chemiluminescence. The same blot was probed with Ponceau S.

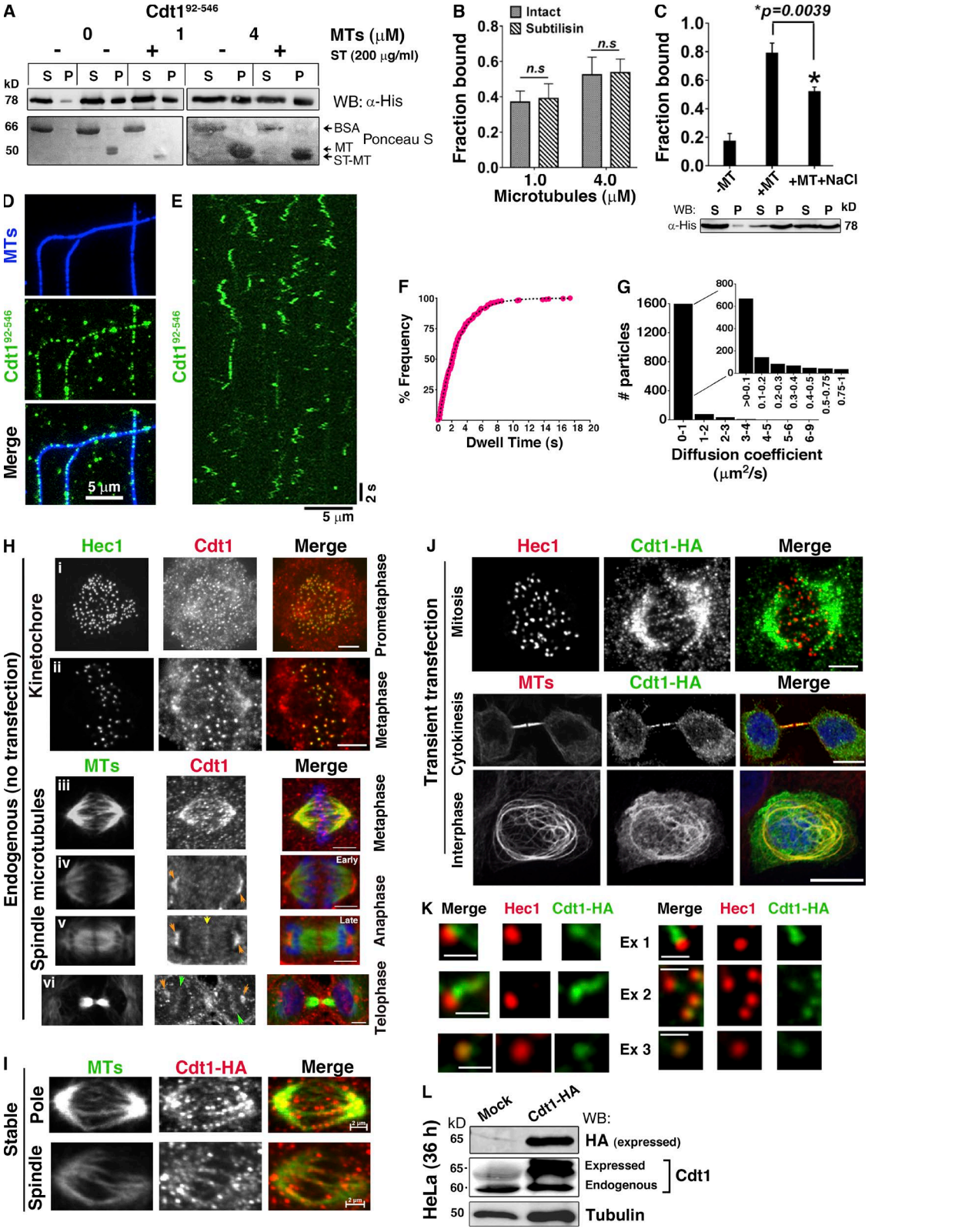

Figure 2. **Cdt1 diffuses on MTs in vitro and decorates spindle MTs in vivo. (A)** Representative Western blot of Cdt1$^{92–546}$ (1 μM) cosedimentation with intact (MT) or subtilisin-treated (ST-MT) microtubules at 1 and 4 μM concentrations. **(B)** Quantification of A (mean ± SD, *n* = 3). Significance assessed by the two-sided unpaired nonparametric Student's *t* test. **(C)** Quantification of cosedimentation of Cdt1$^{92–546}$ (1 μM) with 16 μM MTs in the absence (+MT) and presence (+MT+S; top) of 250 mM NaCl; mean ± SD, *n* = 3. P < 0.005 represents statistical significance as assessed by the two-sided unpaired nonparametric Student's *t* test. Representative Western blot shown (bottom). **(D)** Single-channel and merged TIR-FM images showing surface immobilized Dylight405-labeled MTs (blue) and GFP-tagged Cdt1$^{92–546}$ (green). **(E)** Kymograph analysis of Cdt1$^{92–546}$ interactions with the MT lattice. **(F)** Cumulative frequency plot and exponential fit of Cdt1$^{92–546}$ dwell times. *n* = 304 molecules, two independent protein preparations. **(G)** Diffusion coefficient analysis of Cdt1$^{92–546}$ on MTs performed using

To lend further support to these observations, full-length Cdt1 was transiently overexpressed with an HA tag in HeLa cells, and immunostaining was performed to assess its localization. In agreement with the results so far, staining with anti-HA clearly reveals localization of Cdt1-HA on the spindle MTs and also on kinetochores (overlap with Hec1, a kinetochore marker required for Cdt1 recruitment) in mitotic cells (Fig. 2 J, top panels; and Videos 2 and 3). As shown in Fig. 2 K, magnification of selected kinetochores from multiple cells further validates Cdt1 localization to kinetochores and kMTs (Fig. 2 K and Videos 2 and 3). Strikingly, interphase cells expressing high levels of Cdt1 showed an MT bundling phenotype (Fig. 2 J). This was not evident in cells with low or moderate expression of Cdt1, which is similar to the previous findings of Welburn et al. (2009), where a bundling phenotype was observed only when GFP-Ska1 was overexpressed in vivo or when a higher concentration of Ska complex was used in vitro. Further, in cells that were undergoing cytokinesis, Cdt1 was localized to MT bundles at the midbody region (Fig. 2 J). Western blotting of transfected HeLa cell lysates with anti-HA (representing the exogenously expressed Cdt1 with HA tag) confirmed expression of Cdt1 as a full-length protein in fusion with the HA tag (Fig. 2 L). Similar MT-staining (spindle/spindle pole) was also obtained in HeLa cells that stably expressed HA-tagged Cdt1, representing a scenario between overexpression and endogenous expression (Fig. 2 I).

Aurora B kinase phosphorylates Cdt1 and affects Cdt1-MT binding in vitro

We then sought to understand how the MT binding of Cdt1 could be regulated. Aurora B phosphorylates multiple substrates at kinetochores to negatively regulate kMT attachments and is also instrumental in correcting erroneous attachments (Welburn et al., 2010; Chan et al., 2012; Schmidt et al., 2012). In vitro studies with purified Ndc80 complex demonstrated that introduction of either multiple phosphorylations or phosphomimetic substitutions within the Hec1 tail reduced Ndc80-MT binding, while a lack of phosphorylation promoted stronger binding (Cheeseman et al., 2006; Umbreit et al., 2012). Similarly, Ska1, another kinetochore-localized MAP, is a substrate for Aurora B, and its phosphorylation at four sites located within the MT-binding domain drastically reduces its kinetochore localization (Welburn et al., 2010; Chan et al., 2012; Schmidt et al., 2012). Mutating two of these, S185 and S242, to aspartate dramatically reduced the MT-binding activity of the Ska complex in vitro and resulted in a mitotic delay and reduced kMT stability in vivo (Welburn et al., 2010; Chan et al., 2012; Schmidt et al., 2012). These aforementioned studies, coupled with the fact that Cdt1 closely resembles the Ndc80 and Ska complexes in being recruited to kinetochores where it binds to spindle MTs and contributes to kMT stabilization (Varma et al., 2012), prompted us to insinuate that Aurora B might be one of the essential kinases involved in regulating Cdt1-MT binding during mitosis.

A close examination of the Cdt1 sequence indeed revealed at least seven putative Aurora B phosphorylation sites (T7, S73, S101, T102, S143, S265, and T358) organized in a canonical Aurora B consensus motif ($(R/K)_{1-3}$-X-(S/T); Meraldi et al., 2004; Fig. 3 A). Five of these seven sites (S73, S101, T102, S143, and S265) have been reported as phosphorylation sites in the literature-curated database (http://www.phosphosite.org and http://www.phosida.org). Because highly conserved S159 in Ska3 was clearly phosphorylated by Aurora B even though it did not match the canonical consensus (Chan et al., 2012), we also included three such sites (T270, T287, and T329) in Cdt1 that were conserved across the species but did not conform to the classic Aurora B sequence motif (Fig. 3 A).

To validate this hypothesis, we first sought to test if Cdt1 is a substrate for Aurora B kinase using an in vitro phosphorylation assay. Under the assay conditions, both myc-tagged full-length hekCdt1 (purified from HEK 293 cells and procured commercially) and vimentin (an established Aurora B substrate [Goto et al., 2003]) were readily phosphorylated by Aurora B (Fig. 3 B). This phosphorylation was markedly reduced upon addition of ZM447439, an Aurora B inhibitor, attesting to its specificity. In tandem, hekCdt1 phosphorylated by Aurora B (using a nonradioactive ATP) was subjected to mass spectroscopy (MS) for identification of phosphosites. The tandem MS (MS/MS) spectra conclusively detected phosphorylation on four Aurora B consensus sites, T7, T102, S143, and T358, uniquely/exclusively in the kinase-treated hekCdt1; with 90% sequence coverage in two independent runs (Fig. S2). S73 and T270 were detected as phosphorylated even in the control hekCdt1 (without the Aurora B kinase), suggesting that these residues can potentially acquire phosphorylation in vivo. Although the S101 and S265 localized on the peptides that were phosphorylated, the exact location of the modified residues could not be designated. The remaining two noncanonical sites, T287 and T329, were unmodified.

Interestingly, Ni^{+2}-NTA agarose-mediated affinity precipitation of HA/His-tagged Cdt1 (from thymidine-synchronized and nocodazole-arrested mitotic cell extracts), but not GFP, led to the coprecipitation of Aurora B kinase as an interacting partner

DiaTrack particle tracking Software. Inset graph shows the histogram distribution of number of particles of $Cdt1^{92-546}$ that diffused on MTs within the range of 0–1 $\mu m^2/s$. **(H)** Untransfected mitotic HeLa cell stained with anti-Cdt1 and either anti-Hec1 antibody (top, panels i and ii) or anti-tubulin antibody (bottom, panels iii–vi). Scale bar, 5 µm. Shown are the representative images for Cdt1 kinetochore (anti-Cdt1/red and anti-Hec1/green) and spindle (anti-Cdt1/red and anti-tubulin/green) staining at different stages of mitosis in HeLa cells as indicated. Orange arrows in panels iv–vi depict Cdt1 staining at the spindle poles; yellow arrow in panel v depicts the Cdt1 staining at the cleavage furrow in late anaphase, and green arrows in panel vi depict Cdt1 localization to the reforming nucleus in telophase. **(I and J)** Immunostaining of stably transfected (I) or transiently transfected (J) HeLa cells with anti-HA, anti-Hec1, and anti-tubulin antibodies, as indicated. Scale bar, 5 µm. The middle and bottom panels in J depict confocal images of cells in cytokinesis and interphase, respectively, with DAPI staining of chromosomes in blue. **(K)** Insets from the image stack of the mitotic cell in the top panels of J (left; also see Video 2) with an example from another cell in Video 3 (right). Scale bar, 1 µm. **(L)** Western blot of mock and transfected lysates to probe for Cdt1 (using anti-HA or anti-Cdt1 as indicated) and mouse tubulin as loading control. Expressed, ectopically expressed (with C-terminal 2×-HA, S- and 12×-His-tags; abbreviated as HASH tags); endogenous, endogenous (without tag) Cdt1.

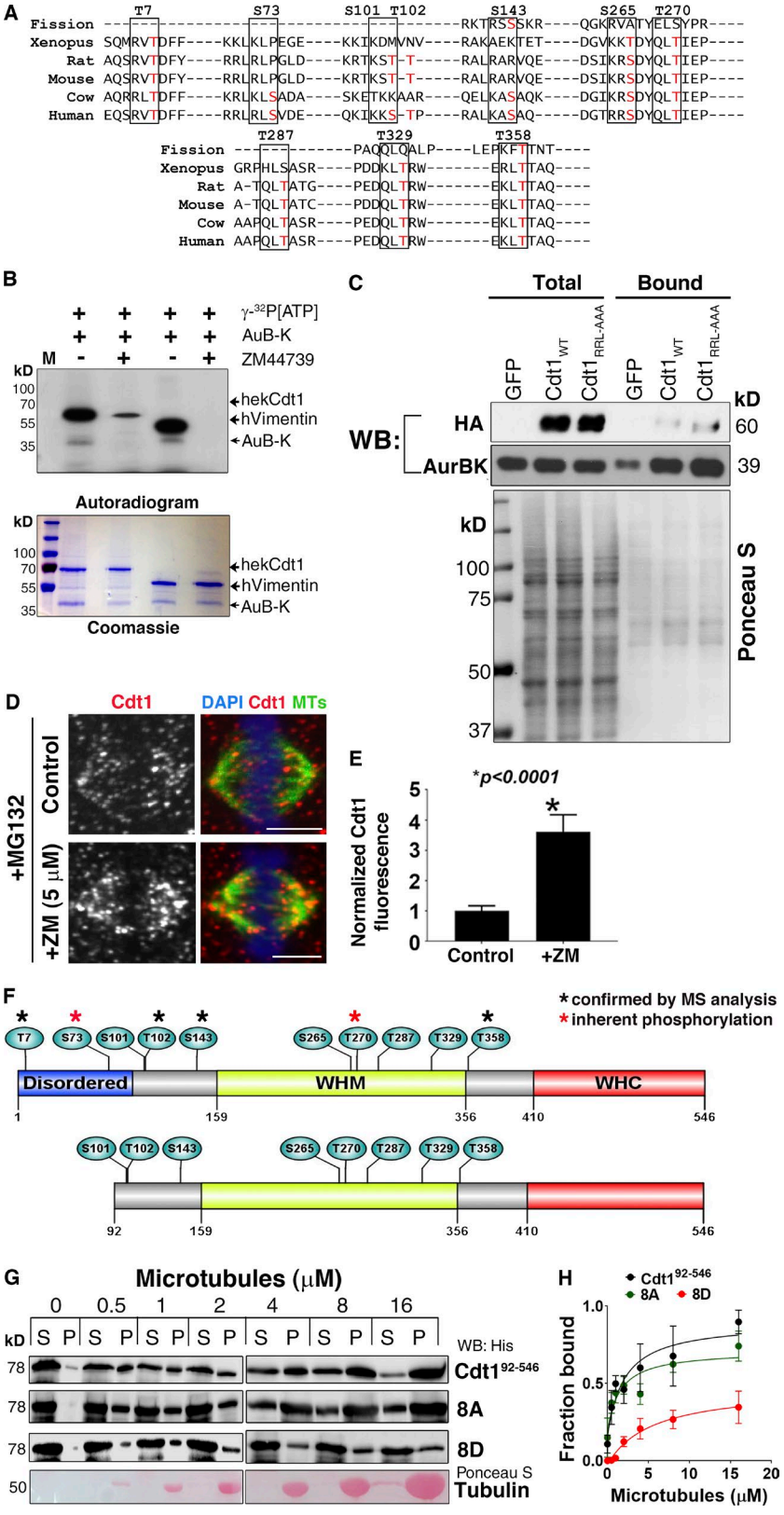

Figure 3. **Aurora B kinase targets Cdt1 for phosphorylation in vitro and affects Cdt1-MT binding.** **(A)** Sequence alignment of Cdt1 from the indicated species using Clustal Omega. Highlighted in the red font are the potential Ser/Thr Aurora B sites. On the top, mentioned are the residues and their positions with respect to the full-length human Cdt1 (1–546 aa). **(B)** In vitro kinase assay with Aurora B alone or kinase plus ZM447439 inhibitor (10 µM) on HEK 293–purified Cdt1 or hVimentin (as a positive control). The autoradiogram (top) and Coomassie-stained gel (bottom) are shown. M, migration of molecular mass standards in kilodaltons on a 12% SDS-PAGE gel. **(C)** Pulldown of Aurora B by HA/His-tagged Cdt1-WT or cy-Cdt1 mutant that blocks cyclin A/Cdk binding (RRL [68–70] AAA), from thymidine synchronized and nocodazole arrested mitotic HeLa cell extracts. The pulldown was performed using Ni^{+2}-NTA agarose beads followed by immunoblotting with either anti-HA or anti–Aurora B (AurB-K) antibodies. 1% of the lysate was loaded as total protein. HEK cells expressing GFP were used as a control. **(D)** HeLa cells were either treated with Aurora B inhibitor, ZM447439 (5 µM), for 1 h or left untreated (control) followed by release into MG132 (10 µM) containing medium in each case. The cells were immunostained with anti-Cdt1 (red), anti-tubulin (green) antibodies and counterstained with DAPI to mark the chromosomes (blue); scale bar, 5 µm. **(E)** n = 10 cells were quantified to obtain normalized Cdt1 fluorescence intensities on spindle MTs as depicted in D. $P < 0.0001$ represents statistical significance as assessed by the two-sided unpaired nonparametric Student's t test. **(F)** Schematic representation showing the full-length Cdt1 (546 aa) and its deletion variant devoid of N-terminal 92 aa generated in fusion with GFP tag for expression in bacteria. The following two proteins generated represent Aurora B phosphomimetic (8D, Ser/Thr substituted with Asp) and phospho-deficient (8A, Ser/Thr substituted with Ala) Cdt1 mutants. Black asterisk, confirmation of phosphosites by mass spectrometry; red asterisk, residues that were inherently phosphorylated in Cdt1 obtained from HEK 293 cells. **(G)** Representative Western blot is shown. Samples fractionated as supernatant (S) and pellet (P) analyzed by Western blot probed with antibody against 6×-His tag to detect Cdt1 and stained with Ponceau S for tubulin. **(H)** Quantification (mean ± SD, n = 3) showing MT cosedimentation of purified $Cdt1^{92–546}$ or the mutant proteins (1 µM each) with the indicated concentrations of taxol-stabilized MTs (in µM). The 95% CI values obtained for each fit were: B_{max} = 0.34–0.65, K_d = 0.43–10.57 for 8D; B_{max} = 0.36–0.67, K_d = 0–3.22 for 8A.

(Fig. 3 C). Moreover, the kinase was also coprecipitated with the HA-tagged Cdt1 mutant (RRL(68–70)AAA), which was incompetent to bind Cyclin/Cdk, equally efficiently as with the WT Cdt1, implying that the interaction between Cdt1 and Aurora B in mitosis is independent of Cdk phosphorylation (Fig. 3 C).

To test the significance of Aurora B phosphorylation on the MT-binding of Cdt1 in vivo, we treated HeLa cells with Aurora B inhibitor (ZM 447439) and assessed the localization of Cdt1 on mitotic spindle MTs. We observed a 3.6-fold increase in spindle MT-localized Cdt1 in ZM-treated cells compared with the

untreated control cells (Fig. 3, D and E). Consistent with this finding, upon mutating the eight putative Aurora B Ser/Thr residues (8D) to Asp in Cdt1$^{92–546}$ in an attempt to mimic constitutively phosphorylated Cdt1 (Fig. 3 F), we observed ∼2.5-fold reduction in the apparent MT binding as evidenced by an increase in the K_d from 2.03 ± 0.99 µM for the Cdt1$^{92–546}$ to 5.50 ± 2.41 µM for the 8D mutant (Fig. 3, G and H). Substitution of the residues to nonphosphorylatable Ala (8A) did not affect the MT binding, with K_d value comparable to the parental Cdt1$^{92–546}$.

Aurora B–phosphomimetic mutations in Cdt1 affect kMT stability and mitotic progression

To assess the role of Aurora B–mediated phosphorylation for Cdt1-MT binding in vivo, we investigated the function of the Aurora B phosphomimetic and nonphosphorylatable Cdt1 mutants in HeLa cells using an experimental strategy that had been established previously. This approach involves siRNA-based knockdown and rescue of Cdt1 function in double thymidine-synchronized cells specifically in the G2/M phase of the cell cycle to ensure that Cdt1 function in replication licensing during G1 phase is unperturbed (Varma et al., 2012). We first generated HeLa cells stably expressing HA-tagged WT and phosphomutant Cdt1 using a retroviral transduction-based approach. The stability of kMTs in cells that were depleted of endogenous Cdt1 but rescued with Cdt1 WT or phosphorylation site mutants was tested. Upon cold treatment, the expression of Cdt1-WT rescued kMT stability as opposed to that of the phosphomimetic mutant (Cdt1-10D) or the vector control (simulates Cdt1-depleted state; Fig. 4, A and B). However, not only did the nonphosphorylatable mutant (Cdt1-10A) maintain stable kMT attachments, but the quantitation of fluorescence intensities of spindle MTs suggested that the kMTs were also hyperstable in this case (Fig. 4, A and B). Under our conditions, efficient knockdown of endogenous Cdt1 was achieved while the expressed siRNA resistant HA-tagged Cdt1 proteins were retained (Fig. 4 C, top and bottom panels). The cells expressing either the WT or mutant proteins after endogenous Cdt1 depletion had apparently normal spindle structures at 37°C (Fig. S3 A) and no defect in localization of Hec1 to kinetochores (Fig. S3 B).

Approximately 60% of the cells analyzed in Cdt1-10D and 80% in vector control had no discernible MT structures after cold exposure; in the remaining cells that showed extant MT traces, the MTs were not attached to the kinetochores (Fig. 4 A, last panels in each vector and 10D). Quantification of the bi-oriented kinetochores that made contact with cold-stable MTs from opposite spindle poles revealed an ∼90% decrease in cells expressing phosphomimetic Cdt1 compared with cells expressing WT or phospho-defective Cdt1 (Fig. 4 D). The interkinetochore distance (K-K stretch), which serves as another indicator of the strength of kMT attachment, was also measured in each case as another parameter. The average K-K stretch in cells expressing Cdt1-WT and Cdt1-10A was 1.11 ± 0.09 and 1.16 ± 0.15 µm, respectively (Fig. 4 E), implying that kMTs from opposite spindle poles form robust contact with sister kinetochores. In contrast, the Cdt1-10D mutant exhibited a significant reduction in the distance between sister kinetochores (0.73 ± 0.10 µm) similar to the vector control, 0.72 ± 0.08 µm, indicating weakened load-bearing kMT attachments between kinetochore pairs (Fig. 4 E). Magnified images of kinetochore pairs are also shown to underscore the observed effects (i.e., reduction of the K-K distance and occurrence of mono-oriented or unattached KT pairs) in Aurora B phosphomimetic mutant and the vector control (Fig. 4 E).

To conclusively address if expression of Cdt1-10A led to the production of hyperstable kMT attachments, we performed STLC (analogous to Monastrol, an inhibitor of Kinesin Eg5) washout assay to test the ability of cells to correct syntelic attachments (Kapoor et al., 2000). The data revealed that 1 h after drug washout, only ∼38% of cells expressing nonphosphorylatable Cdt1 mutant (10A) had attained bipolar spindle structures, in contrast to ∼76% of cells rescued with the WT-Cdt1 protein (Fig. 4, F and G). Based on the substantial delay in bipolarization of the mitotic spindles and accumulation of either monopolar spindles or early prometaphase-like spindle structures in 10A rescued cells, it is evident that there is some degree of kMT hyperstability associated with the expression of the Cdt1-10A mutant compared with cells rescued with WT-Cdt1.

Progression through mitosis was monitored in each case by fixed-cell analyses. Cells were fixed at two different time points after release from thymidine arrest: mitotic onset (11.5 h) and anaphase onset (12.5 h; Varma et al., 2012). The mitotic progression of cells expressing Cdt1-10D was severely disrupted. Similar to that observed for vector control after the depletion of endogenous Cdt1 (Varma et al., 2012), the Cdt1-10D–expressing cells exhibited a phenotype resembling a mid- to late pro-metaphase arrest at the latter time point (Fig. 4, H and I). In this case, majority of the cells had chromosomes that were partially aligned around a vaguely defined metaphase plate (Fig. S3 A), while a smaller fraction of cells exhibited substantially higher levels of chromosome misalignment (not depicted). These phenotypes were strikingly different from the cells expressing the Cdt1-10A mutant, which underwent anaphase onset and cytokinesis similar to the cells rescued with Cdt1-WT.

Although we did not demonstrate that these 10 sites in Cdt1 could be phosphorylated by Aurora B kinase in vivo, MS data unequivocally confirmed at least four target residues (T7, T102, S143, and T358) that were phosphorylated by Aurora B in vitro. Therefore, to evaluate whether mutating the four identified sites is sufficient to recapitulate some or all of the observed phenotypes (especially perturbation of kMT stability and mitotic progression), we generated HeLa cells stably expressing siRNA resistant versions of HA-tagged phosphomimetic (4D) and nonphosphorylatable (4A) mutant Cdt1 proteins. Using the aforementioned siRNA-based knockdown-rescue approach, kMT cold stability and fixed-cell mitotic progression analyses were conducted for these mutants as well. Results from the cold stability experiment indicate that cells rescued with the expression of Cdt1-4D mutant after the depletion of endogenous Cdt1 still exhibited substantial loss of kMT stability compared with the cells rescued with WT-Cdt1, even though the effects were not as severe as those observed in cells expressing Cdt1-10D mutant (Fig. 5 A). Consequently, the incidence of unattached or mono-oriented kinetochores after Cdt1-4D expression was intermediate/partial with respect to Cdt1-WT– and Cdt1-10D–expressing cells. Interestingly, the cells expressing Cdt1-4A also displayed a significant

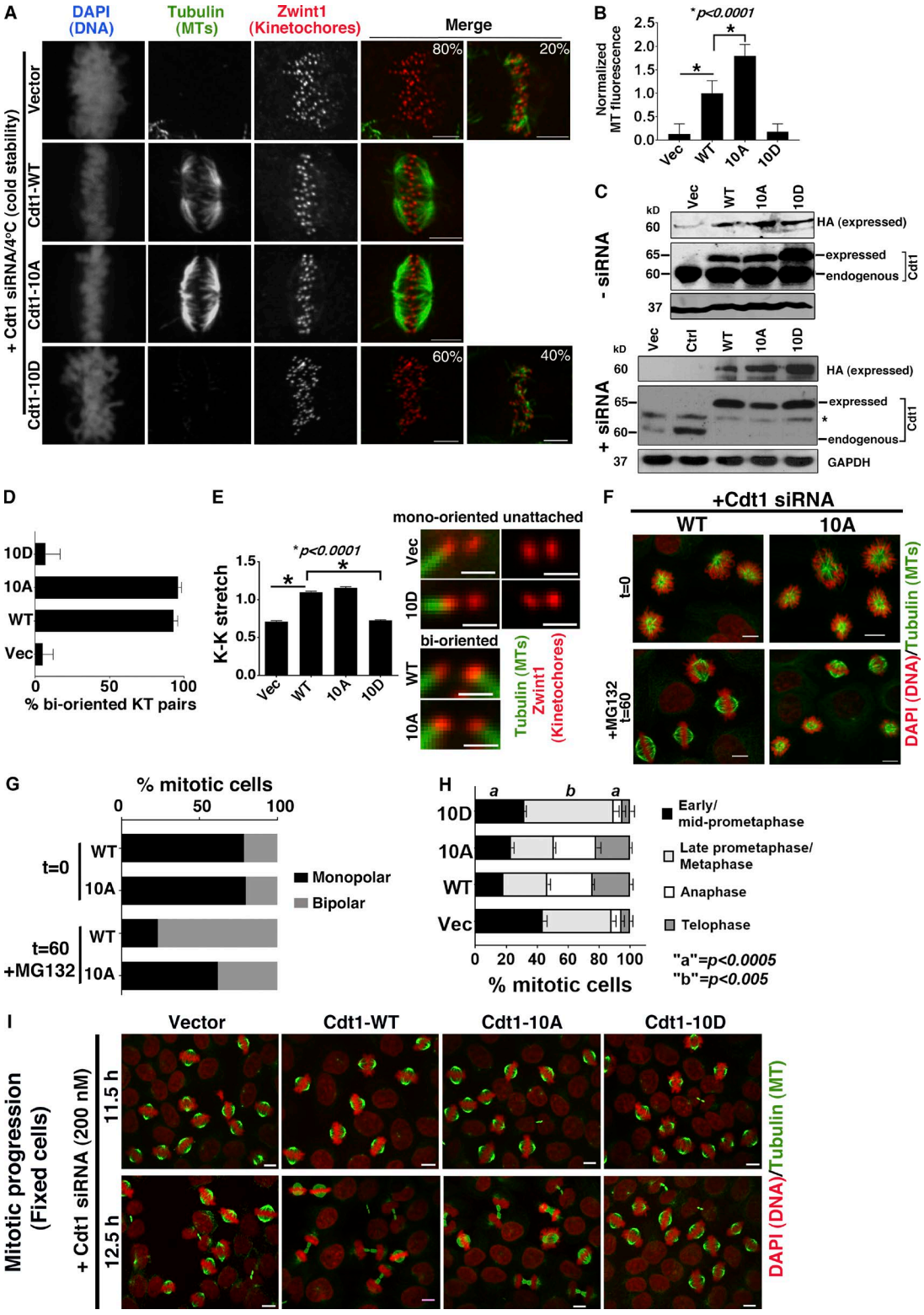

Figure 4. **Aurora B phosphorylation of Cdt1 regulates kMT stability and mitotic progression. (A)** Synchronized HeLa cells treated with siRNA against endogenous Cdt1 in G2/M phase and rescued with stably expressing siRNA-resistant Cdt1-WT, 10D (phosphomimetic), 10A (unphosphorylated) proteins or vector control (abbreviated as Vec, simulating Cdt1 depleted state); were stained with antibodies against Zwint1 in red (1:400 dilution, kinetochore marker), MTs in green (1:500 dilution, spindle marker), and DAPI in black and white marking the chromosomes. Cells were placed at 4°C for 15 min before being fixed and stained. Scale bar, 5 µm. **(B)** Bar graph showing the quantification of MT staining intensity in each case after background subtraction (n = 10 cells). $P < 0.0001$ represents statistical significance as assessed by the two-sided unpaired nonparametric Student's t test. **(C)** HeLa cells treated with siRNA against endogenous Cdt1 rescued with stably expressing siRNA-resistant Cdt1-WT, 10D (phosphomimetic), 10A (phosphodefective) proteins (with C-terminal HASH tags) or vector control (Vec) were lysed using 2× Laemmli buffer and electrophoresed on 10% SDS-PAGE gel. Representative Western blots from three independent experiments of synchronized HeLa cell lysates probed for expression levels of the indicated proteins with (bottom) or without (top) Cdt1 siRNA (200 nM).

increase in the stability of kMTs compared with the Cdt1-WT, but to a significantly lesser extent than the cells expressing the Cdt1-10A mutant (Fig. 5 B). Mitotic progression analysis corroborates the above data, as cells rescued with Cdt1-4A/4D exhibited phenotypes of intermediate severity between the Cdt1-WT expression and the more penetrant, 10A/10D mutant expression (Fig. 5, C and D). As previously described, the cells were fixed at two different time points, mitotic onset (11.5 h) and anaphase onset (12.5 h). Although fewer mitotic cells expressing Cdt1-4A were able to enter anaphase compared with those expressing Cdt1-10A at 12.5 h, there was a significant increase in the number of mitotic cells expressing Cdt1-4D that were able to enter anaphase compared with the Cdt1-10D expressing cells (Fig. 5, C and D). In support of the in vivo analysis, an MT copelleting assay was also performed with the 3D mutant in which three of four identified sites in $Cdt1^{92–546}$ were substituted with Asp to mimic constitutively phosphorylated Cdt1 (Fig. 5 E). The apparent K_d of the 3D mutant for MTs was calculated to be 3.27 ± 0.66 µM, as opposed to 1.85 ± 0.34 µM for $Cdt1^{92–546}$, indicating an ∼1.5-fold reduction in the MT-binding ability of the 3D mutant (Fig. 5, F and G).

We performed live-cell imaging to substantiate our data from fixed-cell mitotic progression. However, for this analysis, we chose Cdt1-10A and -10D mutants since they yielded a more complete and potent phenotype. The vector control and cells rescued with Cdt1-WT or -10A or -10D Aurora B mutant versions were subjected to live imaging after the knockdown of endogenous Cdt1 (Fig. 6 A and Videos 4, 5, 6, and 7). Hoechst was used to mark the chromosomes before the initiation of live imaging. Because there was no noticeable delay in the alignment of the majority of chromosomes in any of the four samples, we quantified the time elapsed between the initial establishment of the metaphase plate and the final fate of each of the imaged mitotic cells. We found that ∼100% of the Cdt1-WT rescued mitotic cells underwent normal anaphase onset without any delays (n = 26/27; Video 4), while >80% of the vector control (n = 22/27; Video 5) and the Cdt1-10D rescued cells (n = 23/28; Video 6) exhibited prolonged mitotic arrest with a metaphase-like chromosome alignment. In the latter two conditions, the aligned state of the chromosomes was (a) maintained for an extended period of time until the last time point of live imaging (outcome 1); (b) followed by anaphase onset with chromosome missegregation events (outcome 2); or (c) disrupted by chromosomal decondensation and reversion to an interphase-like stage (outcome 3). More importantly, vector control and the Cdt1-10D–expressing mitotic cells, on average, took approximately three times longer (∼200 min) to reach their final fate (outcomes 1, 2, and 3 above), with ∼15% cells never progressing into anaphase (outcome 1; Fig. 6 B and Videos 5 and 6). Even though 10A mutants progressed through mitosis comparably to the WT-rescued cells, >50% of these cells (n = 15/28; Video 7) underwent chromosome missegregation events during anaphase, which we speculate is a consequence of hyperstable kMT attachments.

Discussion

In this study, we demonstrate that the DNA replication licensing protein Cdt1, which is recruited to mitotic kinetochores by the Ndc80 complex (Varma et al., 2012), also binds to MTs directly in a manner that its affinity is controlled by Aurora B kinase phosphorylation. The affinity of Cdt1 for MTs was found to be comparable with other relevant kinetochore MAPs such as chTOG (Spittle et al., 2000), Ska (Schmidt et al., 2012), the KMN network, and the Ndc80 complex (Cheeseman et al., 2006; Ciferri et al., 2008) computed using similar approaches. Lack of contribution from the Cdt1's unstructured N-terminal 92 aa in MT binding indicates that the mechanism by which Cdt1 binds to MTs is distinct from the Hec1 subunit of Ndc80, where a positively charged N-terminal 80-aa-long unstructured tail is essential for proper MT binding of the Ndc80 complex (Guimaraes et al., 2008). The fact that the C terminus of Cdt1 (410–546 aa) was not able to bind to MTs alone as effectively as in the presence of N terminus is reminiscent of the pattern obtained with the Ska complex, wherein the removal of C termini from either Ska1 or Ska3 impaired MT binding, but at the same time, the purified C-terminal domains of Ska1 or Ska3 by themselves did not associate with MTs (Jeyaprakash et al., 2012). This suggests that the N terminus of Cdt1 (1–410 aa) may be inert for MT binding by itself but might facilitate the folding or po-

Expressed, ectopically expressed (with HASH tags); endogenous, endogenous (without tag) Cdt1; * in the bottom panel, detection of a nonspecific band reactive with the Cdt1 antibody. The same blot was reprobed with GAPDH (1:8,000) as a sample recovery control. **(D)** Quantification of the percentage of bi-attached, bi-oriented kinetochores in each of the conditions as indicated. Kinetochore marker, Zwint1, is in red, and MT is in green. **(E)** Interkinetochore (K-K) stretch was calculated between the two kinetochore pairs in each case and is plotted (n = 115 pairs; 10 cells). P < 0.001 represents statistical significance as assessed by the two-sided unpaired nonparametric Student's t test. Cropped images of representative kinetochore pairs are also provided to indicate the status of their kMT attachment and K-K stretch; scale bars, 1 µm. **(F)** STLC washout assay was performed in double thymidine synchronized HeLa cells, treated with siRNA against endogenous Cdt1, and rescued with either Cdt1-WT or Cdt1-10A followed by treatment with STLC for 2 h. The cells were washed with and released into medium containing MG132 and fixed either immediately after the initiation of the washout (t = 0) or after 1 h (t = 60), followed by fixation and staining. DAPI is pseudocolored in red to mark chromosomes, and tubulin is in green. **(G)** Bar graph showing the quantification of monopolar (early prometaphase) versus bipolar spindle (metaphase) structures at the indicated time points after STLC washout. Cells from two coverslips in two independent experiments were counted; n = 2,114 and 2,659 for WT and 10A, respectively, for t = 60; n = 565 and 785 for WT and 10A, respectively, for t = 0. The data are plotted as percentage mitotic cells with monopolar or bipolar spindle structures on the y-axis. **(H)** Mitotic progression (metaphase-to-anaphase transition) was assessed in HeLa cells stably expressing vector, Cdt1-WT, Aurora B Cdt1-phosphomimetic (10D) or phospho-defective (10A) mutants at 11.5 and 12.5 h after release from thymidine treatment in the presence of Cdt1 siRNA. The number of cells in each stage of mitosis was counted and plotted from three different coverslips of two independent experiments to illustrate the nature of mitotic delay/arrest in Cdt1-10D mutant–expressing cells compared with cells rescued with Cdt1-WT or Cdt1-10A expression (n = 600 cells; a and b represent the statistical significance obtained using two-sided unpaired nonparametric Student's t test performed on the WT versus 10D in the indicated stages of mitosis). **(I)** Representative images are shown from H; DAPI pseudocolored in red marks the chromosomes, and antibody against tubulin stained the MTs green.

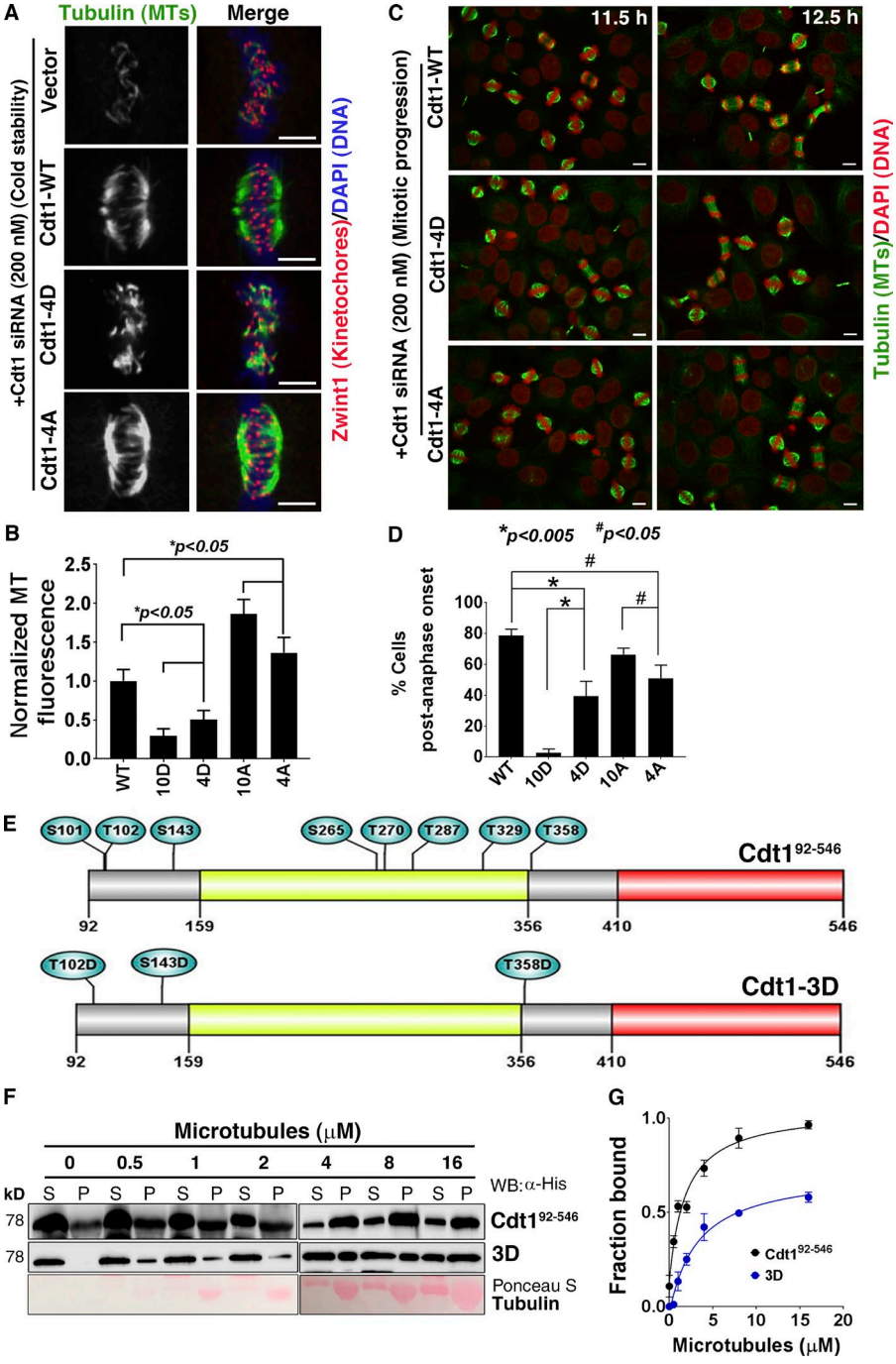

Figure 5. **Aurora B phospho mutants of Cdt1 at the four sites identified by mass spectroscopic analysis partially affect kMT stability and mitotic progression.** Synchronized HeLa cells treated with siRNA against endogenous Cdt1 in G2/M phase and rescued with stably expressing siRNA-resistant Cdt1-WT, 4D (phosphomimetic), 4A (unphosphorylated) proteins or vector control (simulating Cdt1 depleted state) were subjected to 4°C treatment for 15 min before being fixed and stained. **(A)** Representative images of cells from C, immunostained with antibodies against Zwint1 (kinetochore marker) in red, tubulin (MTs) in green or in black and white on the left of the merged images, and DAPI in blue marking the chromosomes. Scale bar, 5 µm. **(B)** Bar graph showing the quantification of spindle MT staining intensity after cold treatment in each case after background subtraction (n = 7). P < 0.05 represents statistical significance as assessed by the two-sided unpaired nonparametric Student's t test. **(C)** Mitotic progression (metaphase-to-anaphase transition) was gauged in HeLa cells stably expressing Cdt1-WT, Cdt1-10D, Cdt1-10A, Cdt1-4D, and Cdt1-4A mutants at 11.5 and 12.5 h after release from thymidine treatment in the presence of Cdt1 siRNA (200 nM). Representative images are shown from E; DAPI pseudocolored in red marks the chromosomes, and antibody against tubulin stained the MTs green; scale bar, 10 µm. **(D)** The number of cells in each stage of mitosis was counted and plotted from three different coverslips to illustrate the difference in mitotic delay in Cdt1-4A/4D mutant–expressing cells compared with cells rescued with Cdt1-WT or Cdt1-10A/10D expression (n = 300); * and #, P values showing the statistical significance among the indicated groups obtained using two-sided unpaired nonparametric Student's t test. **(E)** Schematic representation showing the three indicated Aurora B sites mutated to generate a 3D phosphomimetic mutant in the Cdt1$^{92–546}$ parental background. **(F)** Representative Western blot from a MT-cosedimentation experiment performed with Cdt1$^{92–546}$ and Cdt1-3D mutant is also shown. Samples fractionated as supernatant (S) and pellet (P) analyzed by Western blot probed with antibody against 6×-His tag to detect Cdt1 (WT or 3D mutant) and stained with Ponceau S for tubulin. **(G)** Quantification (mean ± SD, n = 3) showing MT cosedimentation of purified Cdt1$^{92–546}$ or the mutant proteins (1 µM each) with the indicated concentrations of taxol-stabilized MTs (in µM). The 95% CI values obtained for each fit were: B_{max} = 0.8–1.0, K_d = 1.22–2.90 for Cdt1$^{92–546}$; B_{max} = 0.67–0.85, K_d = 2.25–4.9 for 3D mutant.

sitioning of the C terminus of Cdt1 to allow MT binding. Moreover, we predict that WHC or WHM domains may be required in combination for efficient binding of Cdt1 to MTs. These observations also suggest that the WHD domain could serve as one of the conserved MT-binding domains in such proteins, as has already been demonstrated for the Ska complex (Schmidt et al., 2012; Abad et al., 2014). Further, it is interesting that although the N-terminal region of Cdt1 could not bind to MTs, it was competent enough to interact with Hec1; thus it seems that Cdt1 modular functions (Hec1 and MT binding) are independent of each other even though Ndc80 loop is essential for recruiting Cdt1 to the kinetochores.

Additionally, our study demonstrates for the first time that Cdt1 is a substrate for Aurora B kinase and provides evidence for a physical interaction between the two proteins in vivo. However, in the pulldown experiment, we found that the amount of tagged

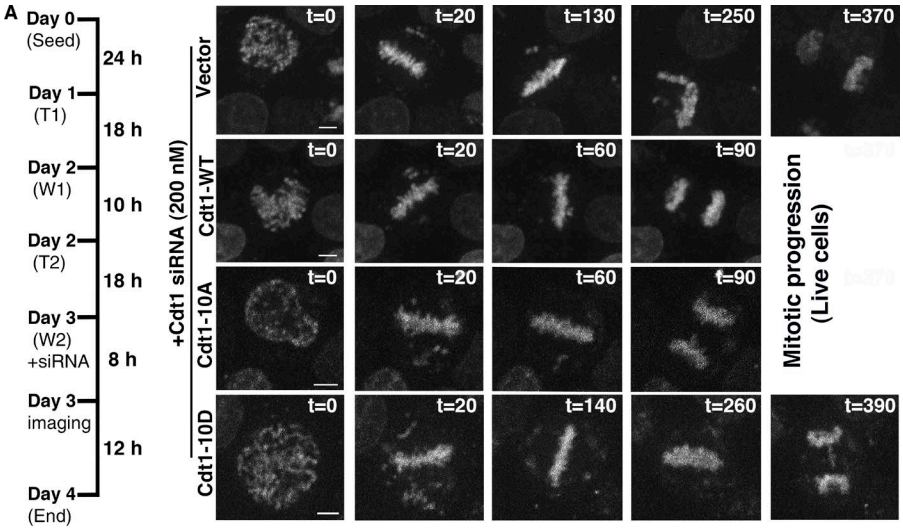

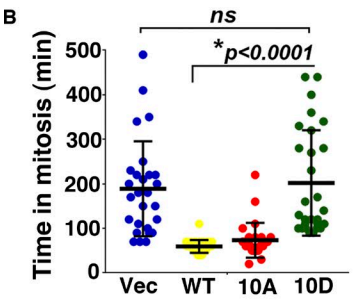

C

	hNdc80	hSka	hCdt1
MT binding	+	+	+
K_d (μm)	Variable	2.5	2.2
Diffusion ($\mu m^2/s$)	$0.03_{Broccoli}$ 0.078_{Bonsai}	0.18	0.16
ΔE-hooks	Reduced	Unaffected	Unaffected
Motif/domain	CH/tail	WTH	WHM/C?
Region	N-ter.	C-ter./132-255 aa	C-ter./central?
MT-type	Straight	Straight/curved	Straight/curved
Kinase	ABK	ABK, Cdk1, Mps1	ABK, MAPK?, Cdk1? Mps1?

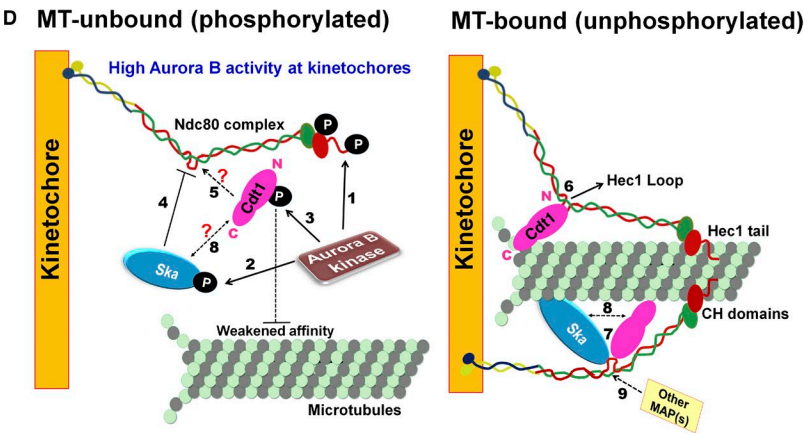

Figure 6. **Live-cell imaging analysis of cells rescued with Aurora B phosphomimetic Cdt1 mutant reveals a severe delay in mitotic progression. (A)** Scheme of the time course and still images obtained at the indicated time points during the imaging of live mitotic progression in different stable cell lines rescued with either the plasmid vector (analogous to Cdt1 depletion) or by WT or Aurora B mutant Cdt1 expression. Chromosomes are marked with Hoechst dye. (See also Videos 4, 5, 6, and 7.) **(B)** Quantification of A. Time (in min) elapsed between the establishment of a metaphase plate and the final fate of each of the imaged mitotic cells, which included delayed anaphase onset or a prolonged mitotic arrest, was plotted on the y-axis for each of the samples imaged live as indicated. Statistical significance assessed by the two-sided unpaired nonparametric Student's *t* test. **(C)** Comparative tabulation of MT-binding parameters and phospho-regulation of relevant kinetochore-associated proteins from vertebrates. **(D)** Working model depicting the role of Cdt1 in providing an additional kMT-attachment site besides the CH and the N-terminal tail domain of the Hec1 subunit of the Ndc80 complex. The CH domains in Hec1 and Nuf2 along with the Hec1 unstructured tail bind MTs. The unstructured ∼40-aa loop region of Hec1 recruits Cdt1 by interacting with the N-terminal 1–320 aa of Cdt1 (Varma et al., 2012). This induces a conformational shift in the Ndc80 complex in a manner that is dependent on Cdt1 binding to MTs. In prometaphase, when kinetochores are not bi-oriented, Aurora B kinase is active to destabilize the erroneous attachments by phosphorylating several kinetochore proteins including Ndc80 (1), Ska (2), and Cdt1 (3) shown in the present study, all of which bind to MTs. Upon phosphorylation, these proteins exhibit reduced affinity for MTs. As observed for the Ska complex, which cannot interact with the KMN network effectively upon its phosphorylation by Aurora B (4); whether Cdt1~P can dock on to the Hec1 loop (5) with similar efficiency to unphosphorylated Cdt1 is still undetermined. In metaphase, when the Aurora B gradient diminishes at kinetochores, Cdt1 becomes proficient to bind to MTs (6), thus providing an additional site for kMT attachment besides the CH and the tail domains of Ndc80. Whether Cdt1 can interact with the Ska complex in its free or loop-bound state and if this interaction is dependent on their phosphorylation status (7 and 8) is yet to be determined. The model also depicts the possibility of interaction of other MAPs with the Hec1 loop, either alone or with the help of Cdt1 or Ska or both (9), as shown using dashed arrows.

Cdt1 retrieved/bound (Fig. 3 C, WB: HA, lanes 5 and 6) was much less compared with the "total" protein expressed (lanes 2 and 3). This is because the polyhistidine tag used to retrieve Cdt1 binds to nickel resin very specifically but extremely poorly in the incompatible buffer conditions used, essentially to preserve and retain Cdt1 binding partners. Nonetheless, endogenous Aurora B kinase was associated significantly above the background control in each case. In addition to Aurora B kinase, Cdt1 has been shown to be phosphorylated by cyclin-dependent kinase 1 (Cdk1) during the S-phase at threonine 29 (Fujita, 2006) and by MAPK p38 and JNK during G2/M phase (Chandrasekaran et al., 2011). Fairly recently, Ska3 has also been shown to undergo Cdk1-mediated phosphorylation that influences its interaction with the Ndc80 loop domain (Zhang et al., 2017). Mps1 kinase was shown to phosphorylate both Ska3 (Maciejowski et al., 2017) and the yeast Ndc80 complex (Kemmler et al., 2009), in addition

to a physical interaction with human Ndc80 (Nilsson, 2015). For Hec1, although Aurora B is regarded as the master regulator, the involvement of Aurora A kinase in late mitosis has lately been uncovered (DeLuca et al., 2018). With this ever-growing evidence of spatio-temporal integration of several mitotic kinases to fine-tune kMT stability, attachment error correction, and mitotic progression, we envision a similar interplay of kinases in regulating mitotic functions of Cdt1, besides Aurora B.

Nevertheless, we extended our study to understand the implications of Aurora B kinase–mediated phosphorylation on MT-binding ability of Cdt1. Indeed, our data demonstrated a correlation between the phosphorylation of Cdt1 by Aurora B kinase and MT binding. While the phosphomimetic Cdt1-10D mutant was severely compromised to sustain stable kMT attachments, the Cdt1-10A mutant, on the contrary, exhibited enhanced attachment stability. However, this hyperstability did not translate into any discernible chromosome alignment defects, unlike those observed after Hec1-9A mutant expression (DeLuca et al., 2011). This could be attributed to the specific role of Cdt1 during later stages of mitosis, i.e., at metaphase, where it facilitates stabilization of kMT attachments. This is in contrast to Hec1, where Aurora B–mediated Hec1 phosphorylation is actively involved in error correction during early mitosis. Thus, it is reasonable that hyperstable kMT attachments would lead to defective chromosome alignment in Hec1-9A mutant, but in the case of Cdt1, only translate to erroneous chromosome segregation later during anaphase onset.

In an attempt to identify the exact functional Aurora B sites that can sufficiently mimic the observed phenotypes, we focused on only the four residues that were unambiguously identified by MS analysis. While our results confirm the vital contribution of those four Aurora B sites, phosphorylation on some or all of the other remaining sites seems requisite to attain the complete gamut of the phenotype pertinent to kMT stability. In light of the severity of phenotype obtained with the 10D mutation, the possibility of a complete loss of mitotic function for this protein cannot be completely ruled out. It is intriguing that these 10 predicted Aurora B sites are located within the N-terminal unstructured and central WHM (1–410 aa) of Cdt1 that did not show direct association with MTs but somehow seem to contribute to efficient Cdt1-MT interaction (Fig. 1, G and I). Because many of these sites are clustered in regions that are predicted to be disordered, we surmise that Aurora B phosphorylation might induce a conformational change in Cdt1 to regulate its MT-binding ability. This mode of regulation can exist in addition to or in parallel to the manner in which Aurora B phosphorylation generally modulates the affinity of binding; i.e., by interfering with the electrostatic interactions through introduction of multiple negative charges. Unlike Hec1, where multiple Aurora B target sites are grouped in tandem within the small unstructured N-terminal tail, sites within Cdt1 are distributed throughout. Thus we propose that one or both of the following could have elicited destabilization of kMT attachments leading to delayed mitotic progression upon Aurora B phosphorylation of Cdt1: (a) addition of multiple negative charges and (b) a conformational shift.

The behavioral parameters and regulatory aspects of the key MT-binding proteins that participate in stabilizing kMT attachments (including Cdt1) at the vertebrate kinetochores are summarized in Fig. 6 C. Based on our observations, we propose a model in which kinetochore-localized Cdt1 provides another MT-binding site for the Ndc80 complex at its loop domain, thus shedding light on the importance of Cdt1 and the loop in kMT attachments (Fig. 6 D). We envisage that the loop domain of the Ndc80 complex, either alone or in conjunction with bound Cdt1, might also coordinate with other kinetochore MAPs to confer stronger attachments. Thus, future studies will be required to delineate the details of hierarchical recruitment of kinetochore components by the Ndc80 loop. Our work, while providing an essential missing link in the series of events that take place during the stabilization of kMT attachments in mitosis (Fig. 6 D), also opens up several stimulating questions such as (a) whether the Ndc80 complex has any synergistic influence on Cdt1 binding to MTs; (b) whether Ska and Cdt1 coordinate for robust kMT attachments, and if so, whether these proteins dock on to the loop as a preformed complex or interact after they are independently recruited at the loop; (c) whether Ska, Ndc80, and Cdt1 can generate a ternary complex for efficient MT binding; (d) whether chTOG, another Ndc80-recruited kinetochore MAP, influences localization of Cdt1 and its interaction with MTs; (e) whether there is cross-talk and/or interplay of several other kinases besides Aurora B kinase to fine-tune the phosphoregulation of Cdt1 in mitosis; and (f) how phosphorylation of Cdt1 with one or many mitotic kinases influences its localization to kinetochores and whether it affects recruitment of other kinetochore-associated proteins directly or indirectly. Answers to these questions will have major impact on the mitosis field in the quest for novel mechanisms that link mitotic kinetochores to spindle MTs and drive accurate chromosome segregation.

Materials and methods

Chemicals, reagents, cell lines, and bacterial strains

Bacterial strains for cloning and expression were grown in Luria–Bertani (LB) broth or agar supplemented with 100 µg/ml ampicillin or 50 µg/ml kanamycin as appropriate. Enzymes for cloning were purchased from New England Biolabs. Custom oligonucleotides and G-blocks were from Integrated DNA Technologies. Sanger DNA sequencing was conducted at the Northwestern University Genomics core facility.

DNA manipulations: Cloning and mutagenesis

Cdt1 gene sequence was codon optimized and synthesized as a linear DNA strand (G-block, IDT) for subsequent cloning procedures. The largest Cdt1 fragment (92–546 aa), deletion variants (92–232, 92–410, and 410–546 aa), Aurora B phosphomimetic mutants (Ser101Asp, Thr102Asp, Ser143Asp, Ser265Asp; Thr270Asp, Thr287Asp, Thr329Asp, Thr358Asp abbreviated as 8D; and Ser-101Asp, Ser143Asp, Thr358Asp abbreviated as 3D), and non-phosphorylatable mutants (Ser101Ala, Thr102Ala, Ser143Ala, Ser265Ala; Thr270Ala, Thr287Ala, Thr329Ala, Thr358Ala abbreviated as 8A) were cloned in fusion with the N-terminal GFP and 6x-His tags using SspI and Gibson cloning in a commercial plasmid procured from Addgene (pET His6 GFP TEV LIC cloning vector [1GFP], plasmid 29663).

For stable transfections, the genes encoding Cdt1 with mutations that represent Aurora B phosphomimetic (Thr7Asp, Ser73Asp, Ser101Asp, Thr102Asp, Ser143Asp, Ser265Asp; Thr270Asp, Thr287Asp, Thr329Asp, Thr358Asp) and non-phosphorylatable (Thr7Ala, Ser73Ala, Ser101Ala, Thr102Ala, Ser143Ala, Ser265Ala; Thr270Ala, Thr287Ala, Thr329Ala, Thr358Ala) versions, abbreviated as 10D and 10A, respectively, harboring C-terminal 2x-HA, Strep-tag, 12x-His tag were cloned in pQCXIP plasmid using custom gene synthesis services (Thermo Fisher Scientific). In addition, Aurora B phosphomimetic (Thr7Asp, Ser101Asp, Ser143Asp, Thr358Asp) and non-phosphorylatable (Thr7Ala, Ser101Ala, Ser143Ala, Thr358Ala) versions, abbreviated as 4D and 4A, with the same tags as above were custom synthesized by Gene Universal.

In silico analyses

Secondary structure prediction

The protocol was based on the work of Seeger et al. (2012). The full sequence of human Cdt1 (Uniprot ID: Q9H211) was input into 10 different secondary structure prediction servers to reduce the bias from any one program. The prediction of disordered regions is based on amino acid composition, charge/hydropathy index, known disordered sequences from crystal/NMR structures, and other empirical methods. The servers included were PSIPRED, IUPRED, PONDR, FoldIndex, s2D, ESpritz, PROFsec, MFD2p, DISCoP, and YASPIN. Relatively stringent cutoff of >75% within each algorithm was used to classify a residue as disordered. The results of each server were converted to a binary output of "folded/unknown" or "disordered" (0 or 1, respectively). The scores were summed and plotted as a function of amino acid number.

Homology modeling

The full sequence of human Cdt1 (Uniprot ID: Q9H211) was input into the Phyre2 (Kelley et al., 2015), I-TASSER (Roy et al., 2010), and SWISS-MODEL (Schwede et al., 2003) homology modeling servers. Models were aligned using the "cealign" plugin on Pymol. The C-terminal W was chosen to align all models. Crystal structures from human WHM domain (PDB ID: 2WVR; De Marco et al., 2009) and mouse WHC domain (PDB ID: 2KLO; Khayrutdinov et al., 2009) were used as templates for the WHDs. Pymol was used to generate protein structure images, and the final figures were generated in Adobe Illustrator.

Recombinant protein expression and purification

For MT copelleting assays, the fusion proteins along with the GFP protein (as a control) were purified from the soluble fraction after overexpression in BL21(λDE3) at 23°C for 18 h in LB medium, using nickel-affinity chromatography. The proteins purified to 85% purity were dialyzed in 20 mM Tris-HCl, pH 8.0, with 300 mM NaCl and stored at −20°C until further use. Full-length Cdt1 (1–546 aa) was purified as a GST-tagged protein using pGEX-5X-1 followed by tag removal per manufacturer's instructions.

Native tubulin was purified from porcine brains as previously described (Williams and Lee, 1982), flash frozen, stored in aliquots in liquid nitrogen, and clarified of aggregates by centrifugation at 100,000 *g* before use. Full-length human Cdt1 (1–546 aa) purified from HEK293 cells with a C-terminal Myc/DDK tag dialyzed in 25 mM Tris-HCl, pH 7.3, 100 mM glycine, and 10% glycerol was purchased from Origene (TP301657).

For TIR-FM assays, GFP-tagged Cdt1, abbreviated as Cdt1$^{92–546}$, was induced in BL21(λDE3) cells at 30°C for 5 h in enriched terrific broth. Cell pellets were flash frozen in liquid nitrogen and stored at −80°C. Cell pastes were lysed via sonication and spun at 35,000 rpm for 45 min. The soluble fraction was incubated with 6 ml of 50% cobalt IMAC resin (TALON; Clontech) for 1 h at 4°C. The beads were washed with 100 ml wash buffer (25 mM Hepes, pH 7.4, 500 mM NaCl, 2.5 mM imidazole, 5% sucrose wt/vol, and 0.5 mM tris(2-carboxyethyl)phosphine [TCEP]) and eluted with 15 ml elution buffer (wash buffer plus 500 mM imidazole). The eluted protein was concentrated to ∼2.5 ml and injected over a Superdex 200 16/60 SEC column (GE Healthcare) in storage buffer (25 mM Hepes, pH 7.4, 500 mM NaCl, 0.5 mM TCEP, and 5% sucrose wt/vol). Purified, folded Cdt1 eluted at ∼65 ml and was monodisperse. The final protein was ∼95% pure via SDS-PAGE. Protein was flash frozen in liquid nitrogen and stored at −80°C until use.

MT copelleting assay

For MT-binding assay, tubulin was polymerized and stabilized in general tubulin (GT) buffer, BRB80 (80 mM Pipes, pH 6.8, 1 mM $MgCl_2$, and 1 mM EGTA) with 100 mM GTP, 20 µM paclitaxel/taxol, and 66% glycerol (assay buffer). The proteins (diluted in BRB80 buffer containing 1 mg/ml BSA) were precleared of any aggregates or debris by ultracentrifugation at 70,000 rpm at room temperature for 30 min. The taxol-stabilized MTs (in varying micromolar concentrations) were incubated with indicated concentrations of precleared proteins or 2 µM GFP/GST alone to a final reaction volume of 40 µl. Reactions were incubated at room temperature for 20 min and ultracentrifuged for 30 min at 60,000 rpm in a Beckman TLA100 rotor at 25°C. The binding was also performed in the presence of salt by adding 300 mM NaCl to the assay buffer. Pellets (P) and supernatants (S) were separated carefully, equal volumes of SDS sample buffer were added, and samples were run on SDS-PAGE and analyzed by Western blotting with anti-His monoclonal antibody (1:5,000; Abcam) or Cdt1 polyclonal IgG raised in rabbit (1:2,000; H-300, sc-28262; Santa Cruz Biotech). Immunoblots were scanned into Adobe Photoshop, and any manipulations to the brightness were applied to the entire image. Densitometry quantification of the bands representing the arbitrary amount of protein in supernatants and pellets was done using ImageJ software (National Institutes of Health). The percentage binding was measured by calculating the ratio of protein in the pellet (P) and the total protein (S + P). The fraction of protein bound was then plotted against the concentration of MTs, and the data were fitted to the single-site saturation nonlinear regression curve (with no nonspecific binding but background and $K_d > 0$ constrain) using GraphPad Prism 6.0. The K_d values generated represent the average and propagated error from at least three independent experiments.

For cosedimentation assays with subtilisin-treated MTs, 20 µM taxol-stabilized MTs were incubated for 30 min at 30°C with 200 µg/ml subtilisin A (Calbiochem), a serine protease that cleaves the C-terminal 10–20 aa from α- and β-tubulin. The

reaction was stopped with 10 mM PMSF, and digested MTs were pelleted (90,000 rpm, TLA100, 10 min, 25°C) and resuspended in the original volume of GT buffer. The assay was then performed as described above.

Curved tubulin oligomers or rings were generated by incubating tubulin with dolastatin (Tocris Bioscience) dissolved in DMSO in a 2:1 molar ratio for 1 h at room temperature in GT buffer supplemented with 6% DMSO. The rings were purified by ultracentrifugation through a cushion of GT buffer with 40% glycerol. The rings were resuspended in the original volume of GT buffer, and assay was performed as described above. Sheared MTs were prepared by passing taxol-stabilized MTs through a 26.5-gauge needle multiple times immediately before the addition to the protein sample. The generation of increased number of ends was confirmed by transmission electron microscopy.

TIR-FM

Flow chambers containing immobilized MTs were assembled as described previously (McKenney et al., 2014). Imaging was performed on a Nikon Eclipse Ti-E microscope equipped with an Andor iXon EM CCD camera; a 100×, 1.49-NA objective and 1.5× tube lens (yielding a pixel size of 106 nm), four laser lines (405, 491, 568, and 647 nm); and using Micro-Manager software (Edelstein et al., 2014). All assays were performed in assay buffer (30 mM Hepes, pH 7.4, 50 nM K-acetate, 2 mM Mg-acetate, 1 mM EGTA, and 10% glycerol), supplemented with 0.1 mg/ml biotin-BSA, 0.5% Pluronic F-168, and 0.2 mg/ml κ-casein. A final concentration of 1 and 5 nM Cdt1$^{92–546}$ was used. Protein samples from two independent purification batches were used to ensure biological reproducibility. Photobleaching tests (Helenius et al., 2006) revealed that the photobleaching rate of this construct under our conditions exceeded the characteristic dwell time by approximately threefold, and thus our dwell-time calculations do not take photobleaching into account. Dwell times were calculated manually from kymographs of individual MTs and plotted in GraphPad Prism 7.0.

For measuring the diffusion coefficient, the TIR-FM imaging time series of Cdt1$^{92–546}$ were first bleach-corrected by histogram matching using ImageJ and saved as 8-bit multi-page TIFF files before being transferred to the DiaTrack 3.04 Pro particle tracking software (http://www.diatrack.org/), which was then used to identify and track GFP particles localized on MTs. The readout for diffusion coefficient obtained from the tracking software was in (pixel)^2/s, and the time interval between individual time frames of the TIR-FM time series was ∼65 ms. Thus, each readout in (pixel)^2/s was first multiplied by the pixel size (0.106 µm), and again by a factor of ∼15.4 (milliseconds to seconds conversion) to obtain final values in (µm)^2/s. The particles that showed high diffusion were excluded for the calculation of the diffusion coefficient (D), along with the stationary particles. This was done because in the time frame used to conduct the analysis, we were unable to ascertain with accuracy whether these particles were indeed bound to and diffusing along MTs.

In vitro phosphorylation assay

In vitro kinase assay was performed on 1 µg each of hekCdt1 and human vimentin (ab73843, Abcam) at 30°C for 1 h in assay buffer containing 25 mM Hepes, 50 mM NaCl, 1 mM DTT, 2 mM EGTA, 5 mM $MgSO_4$, 10 µM ATP, and 5 µCi γ-[^{32}P]ATP (Perkin Elmer) in the presence of 0.5 µg Aurora B kinase (AURKB-231H; Creative BioMart) alone or with its inhibitor ZM447439 (Sigma; 5 or 10 µM as indicated). Samples (30 µl) were then electrophoresed on SDS-PAGE gel and visualized by autoradiography. The same gel was stained with Coomassie to ascertain migration of the proteins.

Sample preparation for MS, liquid chromatography MS/MS, and data analysis

Both nonradioactive kinase-treated and control samples were precipitated overnight at −20°C with 8 volumes of acetone and 1 volume of TCA. The protein was pelleted by centrifugation at 15,000 *g* for 15 min at 4°C. The pellets were washed twice with 200 µl cold acetone, dried, and resuspended in 8 M urea/0.4 M ammonium bicarbonate, then reduced with 4 mM DTT for 30 min at 50°C. Alkylation with 18 mM iodoacetamide was performed at room temperature for 30 min in the dark. The urea was diluted to less than 2 M with ultrapure water followed by addition of sequencing-grade trypsin (Promega) overnight at a ratio of 1:18 (enzyme:substrate). The peptides were desalted using C18 spin columns according to the manufacturer's instructions. Samples were resuspended in 5% acetonitrile (ACN)/0.1% formic acid (FA) to a final concentration of 0.15 µg/µl.

Nano-liquid chromatography MS/MS analyses were performed with a 75 µm × 10.5 cm PicoChip column packed with 3 µm Reprosil C18 beads. A 150 µm × 3 cm trap packed with 3 µm beads was installed in-line. Solvent A consisted of 0.1% FA in water, and solvent B was 0.1% FA in ACN. Peptides were trapped at 5 µl/min for 5 min, then separated at a flow rate of 300 nl/min with a gradient from 5% to 30% B in 95 min. After a 5-min ramp to 60% B, the column was washed at 95% B and reequilibrated to 5% B with a total analysis time of 120 min. Desalted phosphopeptide-enriched fractions were resuspended in 5% ACN/0.1% FA. 6 µl (0.9 µg) was injected in duplicate for each sample.

The LC was coupled by electrospray to a Q-Exactive HF mass spectrometer operating in data-dependent MS/MS mode with a top-15 method. Dynamic exclusion was set to 60 s, and charge 1+ ions were excluded as well. MS^1 scans were collected from 300–2,000 m/z with resolving power equal to 60,000 at 400 m/z. The MS^1 AGC was set to 3 × 10^6. Precursors were isolated with a 2.0 m/z isolation width, and the HCD normalized collision energy was set to 35%. The MS^2 AGC was set to 10^5 with a maximum ion accumulation time of 120 ms, and the resolving power was 30,000.

MS raw files were searched against the human SwissProt database (version downloaded 8/2016, 20,191 sequences) using the Mascot search engine. Cysteine carbamidomethylation was a fixed modification, and the variable modifications were oxidized methionine, acetylation of protein N terminus, deamidation of Asn/Gln, and phosphorylation of Ser, Thr, and Tyr residues. Two missed cleavages were allowed. Statistical cutoffs and data visualization were accomplished using Scaffold Q+ software (Proteome Sciences). Proteins were selected with a 1% false discovery rate cutoff, and peptides with a 90% identification probability or better were considered. All phosphopeptide spectra were inspected

manually to determine whether the phosphate group had been assigned to the correct amino acid.

Cell culture methods

Transient or stable transfections, immunofluorescence, and confocal microscopy

HeLa or HEK 293 cells were cultured at 37°C with 5% CO_2 in DMEM (Life Technologies) containing 10% FBS (Seradigm, VWR Life Science), 100 U/ml penicillin, and 1 µg/ml streptomycin.

Before transfection, cells were seeded overnight onto 18-mm circular coverslips to achieve ∼60–70% confluence. The cells were then transfected with 0.5 µg pJC13-Cdt1-HASH plasmid (carrying C-terminal tags: 2x-HA, Strep-tag, 12x-His tag followed by a stop codon; gift from J. Cook, University of North Carolina, Chapel Hill, NC) using Effectene transfection reagent (Qiagen) according to the manufacturer's protocol. After 36 h, the cells were fixed in PBS, pH 7.2, containing 4% formaldehyde followed by staining with antibody against the HA tag (1:100; H6908; Sigma), tubulin monoclonal antibody (1:500; T9026, clone DM1A; Sigma), and DAPI dihydrochloride (1:10,000; Life Technologies). Alexa Fluor 488–, Rhodamine Red-X–, or Cy5-labeled donkey secondary antibodies used at 1:250 dilution each were obtained from Jackson ImmunoResearch Laboratories.

To generate stable cell lines, pQCXIP, a bicistronic retroviral expression vector, was used (Julius et al., 2000). Upon transfection into HEK-293T packaging cell line, this vector integrates and stably expresses a viral genomic transcript containing the CMV immediate early promoter, gene of interest, internal ribosome entry site (IRES), and the puromycin resistance gene (Pur^R). The gene of interest and the puromycin resistance gene are cotranscribed, via the IRES, as a bicistronic message (Adam et al., 1991; Goshima and Yanagida, 2000). HEK-293T cells were seeded at a density of 0.75×10^6 in a 10-cm dish. A three-plasmid transfection system was used that contains carrier pQCXIP plasmid (5 µg) expressing the gene of interest (*cdt1*-WT or 10D or 10A) along with the two helper plasmids pVSV-G, 1.25 µg (Clontech) and pCL-eco, 3.75 µg (Imagenex) encoding the Env and Gag/Pol proteins required for virus production. The HEK cells were transfected using calcium phosphate for 48 h, and the culture supernatant containing viral particles was harvested and passed through a 0.45-µm syringe filter. Fresh medium was added to the dish for a second round of collection at 72 h. Next, polybrene (8 µg/ml) was mixed with the filtered virus followed by addition of the virus to the target HeLa cells (seeded at a density of 6.5×10^4 in a 10-cm dish) for 6 h. Selection for the stably integrated cells was performed for 2 wk by addition of 1 µg/ml puromycin, a concentration determined to kill 100% of control untransduced HeLa cells.

For image acquisition, the coverslips were mounted using ProLong Gold Antifade reagent (Invitrogen), and 3D stacks were obtained sequentially at 200-nm steps along the z-axis through the cell using a high-resolution inverted microscope (Eclipse TiE; Nikon) equipped with a spinning disk (CSU-X1; Yokogawa Corporation of America), an Andor iXon Ultra888 EMCCD camera, and a 60× or 100× 1.4-NA Plan-Apochromatic DIC oil immersion objective (Nikon). The images were acquired and processed using NIS Elements software from Nikon.

siRNA transfections, double-thymidine synchronization, and cold stability assay

HeLa cells were synchronized by treatment with 2 mM thymidine for 18 h followed by release for 9 h and then retreatment with 2 mM thymidine for 18 h. Synthetic duplexed RNA oligonucleotide (siRNA) against Cdt1 was transfected into HeLa cells according to the manufacturer's instructions as described previously (Varma et al., 2012) during the second thymidine release and before fixing the cells at designated time points, as indicated in Fig. 4 its legend. Western blot was performed using anti-Cdt1 antibody (H-300; Santa Cruz Biotech) to evaluate the efficiency of Cdt1 knockdown. GAPDH was probed for after stripping the same Western blot as loading control. Other cell manipulations included cold treatment for 15 min with ice-cold PBS before fixation.

STLC washout assay

HeLa cells were double-thymidine synchronized, and siRNA against Cdt1 was added as described above. STLC, an analogue of monastrol (7 µM; Sigma) was added to the cells. After 2 h, cells were either fixed ($t = 0$) or washed twice with and released into fresh medium containing MG132 for 1 h ($t = 60$), before fixation and immunofluorescence staining.

Live-cell imaging

HeLa cell vector controls or those expressing either *wt* or Aurora B mutant versions of Cdt1 cultured on 35-mm glass-bottomed dishes (MatTek Corporation) were subjected to the same thymidine and Cdt1 siRNA treatment regimen described above and imaged live starting at 9 h after release from second thymidine treatment. The chromosomes were labeled with the live cell DNA dye, Hoechst (45 min, 2.5 µg/ml), before the initiation of live imaging. Just before imaging, the Hoechst-containing medium was replaced with prewarmed L-15 medium (Gibco) supplemented with 10% FBS and fresh Cdt1 siRNA mix. Live imaging was carried out using an incubation chamber for microscopes (Tokai Hit Co.) at 37°C and 5% CO_2. Images were recorded using a high-resolution inverted microscope (Eclipse TiE; Nikon) equipped with a spinning disk (CSU-X1; Yokogawa Corporation of America), an Andor iXon Ultra888 EMCCD camera, and a 60× 1.4-NA Plan-Apochromatic DIC oil-immersion objective (Nikon) fitted with an objective heater. Four to six 1.5-µm-separated Z-sections covering the entire volume of the cell were collected every 10 min for up to 12 h. Image processing was performed using NIS Elements.

Ni^2-NTA agarose-mediated pulldown

HEK-293T cells were transfected with the plasmids (Cdt1-HASH or cy-Cdt1 mutant, RRL [68–70] AAA, which prevents Cyclin/Cdk binding, in pQCXIP and pEGFP-N1 as control) for 4 h at 20–30% confluence using PEI max transfection reagent. M-phase synchronization was done by treating the cells with 2 mM thymidine for 18 h, followed by addition of 100 ng/ml (0.33 µM) nocodazole for 10 h. The cells were collected by mitotic shake-off and lysed using lysis buffer (50 mM Hepes, pH 8.0, 33 mM KAc, 117 mM NaCl, 20 mM imidazole, 0.1% Triton X-100, 10% glycerol, 0.1 mM 4-benzenesulfonyl fluoride hydrochloride, 10 µg/ml

pepstatin A, 10 µg/ml aprotinin, 10 µg/ml leupeptin, 1 mM ATP, 1 mM $MgCl_2$, 5 µg/ml phosvitin, 1 mM β-glycerol-phosphate, and 1 mM orthovanadate). The whole-cell lysates expressing the His-tagged proteins were incubated with Ni^{+2}-NTA beads for 3 h with end-on rotation at 4°C. Beads were washed three times with the lysis buffer, and bound proteins were eluted by boiling for 5 min in 40 µl of 2× SDS sample buffer. For immunoblotting, proteins were electrophoresed on SDS-PAGE gels and transferred to PVDF membranes. Immunoblots were developed using chemiluminescence and exposed on x-ray films. Antibodies against Aurora B kinase and HA-tag were procured from Abcam (ab2254) and Sigma (H6908), respectively.

Statistical analysis

GraphPad Prism software (version 7.03) was used for determining statistical significance of the data obtained. A standard nonparametric unpaired two-tailed/sided Student's *t* test was used. This test assumes that both groups of data are sampled from Gaussian populations with the same standard deviation. Data distribution was assumed to be normal, but this was not formally tested.

Online supplemental material

Fig. S1 A shows the topology of a conventional WTH domain; Fig. S1 (B and C) shows that control GST and GFP tags do not bind to MTs; Fig. S1 (D–F) shows Cdt1 binding to straight, curved, and sheared MTs; Fig. S1 G is the TIR-FM image of $Cdt1^{92–546}$ decorating MTs; and Fig. S1 H demonstrates Cdt1 colocalization with MTs in HeLa cells. In Fig. S2 are the chromatograms from phosphoproteomics showing phosphorylation of full-length Cdt1 (1–546 aa) by Aurora B kinase at the indicated residues. Fig. S3 (A and B) demonstrates normal mitotic spindle structure in cells rescued with Aurora B kinase phospho mutants of Cdt1 at 37°C and the localization of Hec1 in these cells. Video 1 shows diffusion of Cdt1 on MTs in TIR-FM. Videos 2 and 3 provide Z-series data of Cdt1-HA colocalization on MTs and kinetochores. Videos 4–7 are live imaging analysis of HeLa cells rescued with Aurora B kinase phospho mutants of Cdt1 after labeling the chromosomes with DNA dye, Hoechst.

Acknowledgments

We thank Dr. Jeanette Cook for the HA-tagged Cdt1 expression plasmid and for valuable intellectual input; Dr. Sarah Rice for constructive suggestions and discussions; Drs. Laimonis A Laimins and Kavi Mehta for providing help with the radioactive experiments; Drs. Arshad Desai and Dhanya Cheerambathur for providing Hec1::Nuf2-His-tagged dimeric complex; Northwestern Genomics Core for DNA sequencing services; and Suchithra Seshadrinathan and Dr. Anita Varma for technical support.

This work was supported by National Cancer Institute grant R00CA178188 to D. Varma and National Institute of Neurological Disorders and Stroke grant R00NS089428 and National Institute of General Medical Sciences grant R35GM124889 to R.J. McKenney.

The authors declare no competing financial interests.

Author contributions: S. Agarwal and D. Varma designed and performed majority of the experiments. K.P. Smith assisted in Cdt1 purification, carried out structural and computational studies, and provided intellectual input. Y. Zhou performed the Cdt1-Aurora B kinase pull down experiment. A. Suzuki performed endogenous Cdt1 antibody staining. R.J. McKenney performed single-molecule TIR-FM experiments. S. Agarwal, R.J. McKenney, and D. Varma analyzed the data. S. Agarwal and D. Varma wrote the manuscript with input from all the authors.

Submitted: 18 May 2017
Revised: 6 February 2018
Accepted: 17 July 2018

References

Abad, M.A., B. Medina, A. Santamaria, J. Zou, C. Plasberg-Hill, A. Madhumalar, U. Jayachandran, P.M. Redli, J. Rappsilber, E.A. Nigg, and A.A. Jeyaprakash. 2014. Structural basis for microtubule recognition by the human kinetochore Ska complex. *Nat. Commun.* 5:2964. https://doi.org/10.1038/ncomms3964

Adam, M.A., N. Ramesh, A.D. Miller, and W.R. Osborne. 1991. Internal initiation of translation in retroviral vectors carrying picornavirus 5′ nontranslated regions. *J. Virol.* 65:4985–4990.

Afreen, S., and D. Varma. 2015. Cell Division: Molecular Pathways for KMN Kinetochore Recruitment. *Curr. Biol.* 25:R332–R335. https://doi.org/10.1016/j.cub.2015.02.041

Chan, Y.W., A.A. Jeyaprakash, E.A. Nigg, and A. Santamaria. 2012. Aurora B controls kinetochore-microtubule attachments by inhibiting Ska complex-KMN network interaction. *J. Cell Biol.* 196:563–571. https://doi.org/10.1083/jcb.201109001

Chandrasekaran, S., T.X. Tan, J.R. Hall, and J.G. Cook. 2011. Stress-stimulated mitogen-activated protein kinases control the stability and activity of the Cdt1 DNA replication licensing factor. *Mol. Cell. Biol.* 31:4405–4416. https://doi.org/10.1128/MCB.06163-11

Cheeseman, I.M., and A. Desai. 2008. Molecular architecture of the kinetochore-microtubule interface. *Nat. Rev. Mol. Cell Biol.* 9:33–46. https://doi.org/10.1038/nrm2310

Cheeseman, I.M., J.S. Chappie, E.M. Wilson-Kubalek, and A. Desai. 2006. The conserved KMN network constitutes the core microtubule-binding site of the kinetochore. *Cell.* 127:983–997. https://doi.org/10.1016/j.cell.2006.09.039

Ciferri, C., S. Pasqualato, E. Screpanti, G. Varetti, S. Santaguida, G. Dos Reis, A. Maiolica, J. Polka, J.G. De Luca, P. De Wulf, et al. 2008. Implications for kinetochore-microtubule attachment from the structure of an engineered Ndc80 complex. *Cell.* 133:427–439. https://doi.org/10.1016/j.cell.2008.03.020

DeLuca, J.G., and A. Musacchio. 2012. Structural organization of the kinetochore-microtubule interface. *Curr. Opin. Cell Biol.* 24:48–56. https://doi.org/10.1016/j.ceb.2011.11.003

DeLuca, K.F., S.M. Lens, and J.G. DeLuca. 2011. Temporal changes in Hec1 phosphorylation control kinetochore-microtubule attachment stability during mitosis. *J. Cell Sci.* 124:622–634. https://doi.org/10.1242/jcs.072629

DeLuca, K.F., A. Meppelink, A.J. Broad, J.E. Mick, O.B. Peersen, S. Pektas, S.M.A. Lens, and J.G. DeLuca. 2018. Aurora A kinase phosphorylates Hec1 to regulate metaphase kinetochore-microtubule dynamics. *J. Cell Biol.* 217:163–177. https://doi.org/10.1083/jcb.201707160

De Marco, V., P.J. Gillespie, A. Li, N. Karantzelis, E. Christodoulou, R. Klompmaker, S. van Gerwen, A. Fish, M.V. Petoukhov, M.S. Iliou, et al. 2009. Quaternary structure of the human Cdt1-Geminin complex regulates DNA replication licensing. *Proc. Natl. Acad. Sci. USA.* 106:19807–19812. https://doi.org/10.1073/pnas.0905281106

Edelstein, A.D., M.A. Tsuchida, N. Amodaj, H. Pinkard, R.D. Vale, and N. Stuurman. 2014. Advanced methods of microscope control using µManager software. *J. Biol. Methods.* 1:e10. https://doi.org/10.14440/jbm.2014.36

Espeut, J., D.K. Cheerambathur, L. Krenning, K. Oegema, and A. Desai. 2012. Microtubule binding by KNL-1 contributes to spindle checkpoint silencing at the kinetochore. *J. Cell Biol.* 196:469–482. https://doi.org/10.1083/jcb.201111107

Fujita, M. 2006. Cdt1 revisited: complex and tight regulation during the cell cycle and consequences of deregulation in mammalian cells. *Cell Div.* 1:22. https://doi.org/10.1186/1747-1028-1-22

Goshima, G., and M. Yanagida. 2000. Establishing biorientation occurs with precocious separation of the sister kinetochores, but not the arms, in the early spindle of budding yeast. *Cell.* 100:619–633. https://doi.org/10.1016/S0092-8674(00)80699-6

Goto, H., Y. Yasui, A. Kawajiri, E.A. Nigg, Y. Terada, M. Tatsuka, K. Nagata, and M. Inagaki. 2003. Aurora-B regulates the cleavage furrow-specific vimentin phosphorylation in the cytokinetic process. *J. Biol. Chem.* 278:8526–8530. https://doi.org/10.1074/jbc.M210892200

Guimaraes, G.J., Y. Dong, B.F. McEwen, and J.G. Deluca. 2008. Kinetochore-microtubule attachment relies on the disordered N-terminal tail domain of Hec1. *Curr. Biol.* 18:1778–1784. https://doi.org/10.1016/j.cub.2008.08.012

Helenius, J., G. Brouhard, Y. Kalaidzidis, S. Diez, and J. Howard. 2006. The depolymerizing kinesin MCAK uses lattice diffusion to rapidly target microtubule ends. *Nature.* 441:115–119. https://doi.org/10.1038/nature04736

Hsu, K.S., and T. Toda. 2011. Ndc80 internal loop interacts with Dis1/TOG to ensure proper kinetochore-spindle attachment in fission yeast. *Curr. Biol.* 21:214–220. https://doi.org/10.1016/j.cub.2010.12.048

Jeyaprakash, A.A., A. Santamaria, U. Jayachandran, Y.W. Chan, C. Benda, E.A. Nigg, and E. Conti. 2012. Structural and functional organization of the Ska complex, a key component of the kinetochore-microtubule interface. *Mol. Cell.* 46:274–286. https://doi.org/10.1016/j.molcel.2012.03.005

Joglekar, A.P., K.S. Bloom, and E.D. Salmon. 2010. Mechanisms of force generation by end-on kinetochore-microtubule attachments. *Curr. Opin. Cell Biol.* 22:57–67. https://doi.org/10.1016/j.ceb.2009.12.010

Julius, M.A., Q. Yan, Z. Zheng, and J. Kitajewski. 2000. Q vectors, bicistronic retroviral vectors for gene transfer. *Biotechniques.* 28:702–708.

Kapoor, T.M., T.U. Mayer, M.L. Coughlin, and T.J. Mitchison. 2000. Probing spindle assembly mechanisms with monastrol, a small molecule inhibitor of the mitotic kinesin, Eg5. *J. Cell Biol.* 150:975–988. https://doi.org/10.1083/jcb.150.5.975

Kelley, L.A., S. Mezulis, C.M. Yates, M.N. Wass, and M.J. Sternberg. 2015. The Phyre2 web portal for protein modeling, prediction and analysis. *Nat. Protoc.* 10:845–858. https://doi.org/10.1038/nprot.2015.053

Kemmler, S., M. Stach, M. Knapp, J. Ortiz, J. Pfannstiel, T. Ruppert, and J. Lechner. 2009. Mimicking Ndc80 phosphorylation triggers spindle assembly checkpoint signalling. *EMBO J.* 28:1099–1110. https://doi.org/10.1038/emboj.2009.62

Khayrutdinov, B.I., W.J. Bae, Y.M. Yun, J.H. Lee, T. Tsuyama, J.J. Kim, E. Hwang, K.S. Ryu, H.K. Cheong, C. Cheong, et al. 2009. Structure of the Cdt1 C-terminal domain: conservation of the winged helix fold in replication licensing factors. *Protein Sci.* 18:2252–2264. https://doi.org/10.1002/pro.236

Lee, C., B. Hong, J.M. Choi, Y. Kim, S. Watanabe, Y. Ishimi, T. Enomoto, S. Tada, Y. Kim, and Y. Cho. 2004. Structural basis for inhibition of the replication licensing factor Cdt1 by geminin. *Nature.* 430:913–917. https://doi.org/10.1038/nature02813

Maciejowski, J., H. Drechsler, K. Grundner-Culemann, E.R. Ballister, J.A. Rodriguez-Rodriguez, V. Rodriguez-Bravo, M.J.K. Jones, E. Foley, M.A. Lampson, H. Daub, et al. 2017. Mps1 Regulates Kinetochore-Microtubule Attachment Stability via the Ska Complex to Ensure Error-Free Chromosome Segregation. *Dev. Cell.* 41:143–156.e6. https://doi.org/10.1016/j.devcel.2017.03.025

Maure, J.F., S. Komoto, Y. Oku, A. Mino, S. Pasqualato, K. Natsume, L. Clayton, A. Musacchio, and T.U. Tanaka. 2011. The Ndc80 loop region facilitates formation of kinetochore attachment to the dynamic microtubule plus end. *Curr. Biol.* 21:207–213. https://doi.org/10.1016/j.cub.2010.12.050

McKenney, R.J., W. Huynh, M.E. Tanenbaum, G. Bhabha, and R.D. Vale. 2014. Activation of cytoplasmic dynein motility by dynactin-cargo adapter complexes. *Science.* 345:337–341. https://doi.org/10.1126/science.1254198

Meraldi, P., R. Honda, and E.A. Nigg. 2004. Aurora kinases link chromosome segregation and cell division to cancer susceptibility. *Curr. Opin. Genet. Dev.* 14:29–36. https://doi.org/10.1016/j.gde.2003.11.006

Nilsson, J. 2015. Mps1-Ndc80: one interaction to rule them all. *Oncotarget.* 6:16822–16823. https://doi.org/10.18632/oncotarget.4837

Pozo, P.N., and J.G. Cook. 2016. Regulation and Function of Cdt1; A Key Factor in Cell Proliferation and Genome Stability. *Genes (Basel).* 8:2. https://doi.org/10.3390/genes8010002

Ramey, V.H., H.W. Wang, Y. Nakajima, A. Wong, J. Liu, D. Drubin, G. Barnes, and E. Nogales. 2011. The Dam1 ring binds to the E-hook of tubulin and diffuses along the microtubule. *Mol. Biol. Cell.* 22:457–466. https://doi.org/10.1091/mbc.e10-10-0841

Roy, A., A. Kucukural, and Y. Zhang. 2010. I-TASSER: a unified platform for automated protein structure and function prediction. *Nat. Protoc.* 5:725–738. https://doi.org/10.1038/nprot.2010.5

Schmidt, J.C., and I.M. Cheeseman. 2011. Chromosome segregation: keeping kinetochores in the loop. *Curr. Biol.* 21:R110–R112. https://doi.org/10.1016/j.cub.2010.12.030

Schmidt, J.C., H. Arthanari, A. Boeszoermenyi, N.M. Dashkevich, E.M. Wilson-Kubalek, N. Monnier, M. Markus, M. Oberer, R.A. Milligan, M. Bathe, et al. 2012. The kinetochore-bound Ska1 complex tracks depolymerizing microtubules and binds to curved protofilaments. *Dev. Cell.* 23:968–980. https://doi.org/10.1016/j.devcel.2012.09.012

Schwede, T., J. Kopp, N. Guex, and M.C. Peitsch. 2003. SWISS-MODEL: An automated protein homology-modeling server. *Nucleic Acids Res.* 31:3381–3385. https://doi.org/10.1093/nar/gkg520

Seeger, M.A., Y. Zhang, and S.E. Rice. 2012. Kinesin tail domains are intrinsically disordered. *Proteins.* 80:2437–2446. https://doi.org/10.1002/prot.24128

Spittle, C., S. Charrasse, C. Larroque, and L. Cassimeris. 2000. The interaction of TOGp with microtubules and tubulin. *J. Biol. Chem.* 275:20748–20753. https://doi.org/10.1074/jbc.M002597200

Tien, J.F., N.T. Umbreit, D.R. Gestaut, A.D. Franck, J. Cooper, L. Wordeman, T. Gonen, C.L. Asbury, and T.N. Davis. 2010. Cooperation of the Dam1 and Ndc80 kinetochore complexes enhances microtubule coupling and is regulated by aurora B. *J. Cell Biol.* 189:713–723. https://doi.org/10.1083/jcb.200910142

Umbreit, N.T., D.R. Gestaut, J.F. Tien, B.S. Vollmar, T. Gonen, C.L. Asbury, and T.N. Davis. 2012. The Ndc80 kinetochore complex directly modulates microtubule dynamics. *Proc. Natl. Acad. Sci. USA.* 109:16113–16118. https://doi.org/10.1073/pnas.1209615109

Varma, D., and E.D. Salmon. 2012. The KMN protein network--chief conductors of the kinetochore orchestra. *J. Cell Sci.* 125:5927–5936. https://doi.org/10.1242/jcs.093724

Varma, D., S. Chandrasekaran, L.J. Sundin, K.T. Reidy, X. Wan, D.A. Chasse, K.R. Nevis, J.G. DeLuca, E.D. Salmon, and J.G. Cook. 2012. Recruitment of the human Cdt1 replication licensing protein by the loop domain of Hec1 is required for stable kinetochore-microtubule attachment. *Nat. Cell Biol.* 14:593–603. https://doi.org/10.1038/ncb2489

Vavouri, T., J.I. Semple, R. Garcia-Verdugo, and B. Lehner. 2009. Intrinsic protein disorder and interaction promiscuity are widely associated with dosage sensitivity. *Cell.* 138:198–208. https://doi.org/10.1016/j.cell.2009.04.029

Wang, H.W., S. Long, C. Ciferri, S. Westermann, D. Drubin, G. Barnes, and E. Nogales. 2008. Architecture and flexibility of the yeast Ndc80 kinetochore complex. *J. Mol. Biol.* 383:894–903. https://doi.org/10.1016/j.jmb.2008.08.077

Welburn, J.P., E.L. Grishchuk, C.B. Backer, E.M. Wilson-Kubalek, J.R. Yates III, and I.M. Cheeseman. 2009. The human kinetochore Ska1 complex facilitates microtubule depolymerization-coupled motility. *Dev. Cell.* 16:374–385. https://doi.org/10.1016/j.devcel.2009.01.011

Welburn, J.P., M. Vleugel, D. Liu, J.R. Yates III, M.A. Lampson, T. Fukagawa, and I.M. Cheeseman. 2010. Aurora B phosphorylates spatially distinct targets to differentially regulate the kinetochore-microtubule interface. *Mol. Cell.* 38:383–392. https://doi.org/10.1016/j.molcel.2010.02.034

Westhorpe, F.G., and A.F. Straight. 2013. Functions of the centromere and kinetochore in chromosome segregation. *Curr. Opin. Cell Biol.* 25:334–340. https://doi.org/10.1016/j.ceb.2013.02.001

Williams, R.C. Jr., and J.C. Lee. 1982. Preparation of tubulin from brain. *Methods Enzymol.* 85(Pt B):376–385. https://doi.org/10.1016/0076-6879(82)85038-6

Zaytsev, A.V., J.E. Mick, E. Maslennikov, B. Nikashin, J.G. DeLuca, and E.L. Grishchuk. 2015. Multisite phosphorylation of the NDC80 complex gradually tunes its microtubule-binding affinity. *Mol. Biol. Cell.* 26:1829–1844. https://doi.org/10.1091/mbc.e14-11-1539

Zhang, G., C.D. Kelstrup, X.W. Hu, M.J. Kaas Hansen, M.R. Singleton, J.V. Olsen, and J. Nilsson. 2012. The Ndc80 internal loop is required for recruitment of the Ska complex to establish end-on microtubule attachment to kinetochores. *J. Cell Sci.* 125:3243–3253. https://doi.org/10.1242/jcs.104208

Zhang, Q., S. Sivakumar, Y. Chen, H. Gao, L. Yang, Z. Yuan, H. Yu, and H. Liu. 2017. Ska3 Phosphorylated by Cdk1 Binds Ndc80 and Recruits Ska to Kinetochores to Promote Mitotic Progression. *Curr. Biol.* 27:1477–1484.e4. https://doi.org/10.1016/j.cub.2017.03.060